nanomaterials

MDPI

Review

Recent Advances in Fabrication of Flexible, Thermochromic Vanadium Dioxide Films for Smart Windows

Jongbae Kim and Taejong Paik *

School of Integrative Engineering, Chung-Ang University, Seoul 06974, Korea; jbkim0406@gmail.com
* Correspondence: paiktae@cau.ac.kr

Abstract: Monoclinic-phase VO_2 (VO_2(M)) has been extensively studied for use in energy-saving smart windows owing to its reversible insulator–metal transition property. At the critical temperature (T_c = 68 °C), the insulating VO_2(M) (space group P21/c) is transformed into metallic rutile VO_2 (VO_2(R) space group P42/mnm). VO_2(M) exhibits high transmittance in the near-infrared (NIR) wavelength; however, the NIR transmittance decreases significantly after phase transition into VO_2(R) at a higher T_c, which obstructs the infrared radiation in the solar spectrum and aids in managing the indoor temperature without requiring an external power supply. Recently, the fabrication of flexible thermochromic VO_2(M) thin films has also attracted considerable attention. These flexible films exhibit considerable potential for practical applications because they can be promptly applied to windows in existing buildings and easily integrated into curved surfaces, such as windshields and other automotive windows. Furthermore, flexible VO_2(M) thin films fabricated on microscales are potentially applicable in optical actuators and switches. However, most of the existing fabrication methods of phase-pure VO_2(M) thin films involve chamber-based deposition, which typically require a high-temperature deposition or calcination process. In this case, flexible polymer substrates cannot be used owing to the low-thermal-resistance condition in the process, which limits the utilization of flexible smart windows in several emerging applications. In this review, we focus on recent advances in the fabrication methods of flexible thermochromic VO_2(M) thin films using vacuum deposition methods and solution-based processes and discuss the optical properties of these flexible VO_2(M) thin films for potential applications in energy-saving smart windows and several other emerging technologies.

Keywords: VO_2; phase change material; flexible thin film; thermochromics; energy efficient materials

Citation: Kim, J.; Paik, T. Recent Advances in Fabrication of Flexible, Thermochromic Vanadium Dioxide Films for Smart Windows. *Nanomaterials* **2021**, *11*, 2674. https://doi.org/10.3390/nano11102674

Academic Editor: Yuanbing Mao

Received: 30 August 2021
Accepted: 5 October 2021
Published: 11 October 2021

1. Introduction

To address the rapidly increasing energy demand and growing environmental concerns, the development of renewable resources and smart-energy materials is receiving widespread attention [1]. Building energy consumption is estimated to account for 30–40% of the total global energy consumption, and this proportion is expected to continue increasing [2,3]. Windows are the most energy-inefficient component of a building; in this regard, smart windows offer the potential to reduce energy consumption by reducing the air-conditioning load via modulation of solar radiation [4]. Researchers have extensively studied the development of energy-efficient materials for smart windows to address the increasing energy needs. Monoclinic-phase VO_2 (VO_2(M)) was first reported by Morin in 1959 and is the most widely studied inorganic material owing to its switchable thermochromic properties [5]. VO_2 exhibits a first-order insulator–metal phase transition at the critical temperature (T_c = 68 °C), accompanied by reversible phase-change properties in the transition from the insulating monoclinic (P21/c) phase to the metallic rutile (P42/mmm) phase [6,7]. Figure 1 shows the crystal structure and band diagram of monoclinic and rutile phase VO_2. The vanadium ions in the monoclinic phase dimerize to form zigzag atomic chains with two V-V distances of ≈3.12 and ≈2.65 Å. Conversely, in the rutile

phase, straight and evenly distanced vanadium chains are formed along the c-axis with ≈2.85 Å of distance and V^{4+} ions surrounded by O^{2-} are located at the center and corner positions [8,9]. Dimerization of the vanadium ion causes the $d_{||}$ band to split into a filled bonding ($d_{||}$) and an empty antibonding ($d_{||}$*). Furthermore, the π* orbitals shift to higher energies and make a forbidden band of approximately 0.7 eV between the $d_{||}$ and π* [10,11]. The Fermi level is located within the forbidden band, thereby forming the insulating VO_2(M). When the temperature is higher than T_c, the density of the Fermi energy states in VO_2(R) is formed by a mixture of π* and $d_{||}$ orbitals [9,12]. The electrons at the $d_{||}$ state exhibit a behavior similar to that of free electrons, accomplishing a half-filled metallic state. The Fermi level form between the π* and $d_{||}$ bands, indicating an enhanced electrical conductivity of the VO_2(R) [13]. Therefore, electrical and optical properties are considerably modulated during the phase transition. The phase transition of VO_2 can be induced by different types of stimuli, such as heat [5], electric fields [14], and mechanical strain [15]. The phase change in VO_2(M) has also been utilized in various emerging technologies, including optical switches [16], thermoelectrics [17], hydrogen storage [18,19], sensors [20–22], transistors [23–25], active metamaterials [26–28], and photoelectric devices [29]. The application of VO_2(M) in smart windows was investigated in the 1980s by Jorgenson et al. [7] and Babulanam et al. [30]. When the external temperature is lower than the phase-transition temperature, which is approximately 68 °C, VO_2(M) exists in the insulating phase, exhibiting high transmittance of near-infrared (NIR) wavelengths in the solar spectrum. Conversely, when the temperature is higher than the phase-transition temperature, the crystal and band structures change because of the transition from the insulator phase (VO_2(M)) to the metallic phase (rutile VO_2 (VO_2(R))), which significantly reduces the optical transmittance of NIR wavelengths. Therefore, thermochromic smart windows can reversibly modulate their solar transmittance at different temperatures and can reduce the room temperature during hot weather conditions; this will reduce the total energy consumption of the building. VO_2-based thermochromic smart windows offer characteristic advantages over other types of energy-saving windows, such as low-emissivity (low-e) glass [31,32] and electrochromic (EC) windows, owing to their ability to self-regulate solar transmission/reflection according to the external environment without utilizing an external energy supply [33–35]. Moreover, thermochromic windows have a relatively simple structure when compared with low-e or EC glass, thereby exhibiting potential for large-area installation and mass production for commercialization [36].

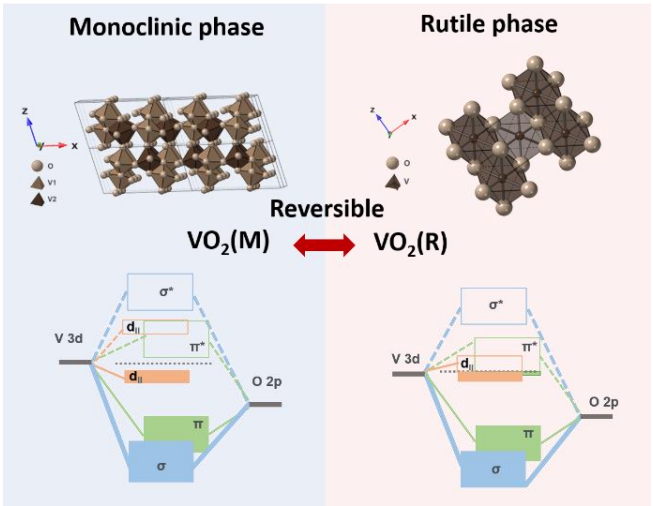

Figure 1. Schematic of the crystal structure and electronic band structure of the insulating VO_2(M) and the metallic VO_2(R). Adapted with permission from [13]. Copyright 2011, American Chemical Society.

The performance of VO_2 for smart windows is evaluated in terms of the luminous transmittance (T_{lum}) and solar modulation ability. Luminous transmittance refers to the

integrated optical amount of visible-light transmittance, which is determined from the following equation:

$$T_{lum} = \int \Phi_{lum}(\lambda)Td\lambda / \int \Phi_{lum}(\lambda)d\lambda, \ (380 \text{ to } 780 \text{ nm})$$

$T(\lambda)$ and Φ_{lum} characterize the transmittance of the wavelength λ and photopic luminous efficiency function in the visible region, respectively [30,37]. Solar-energy modulation ability (ΔT_{sol}) is also a critical feature for determining the energy-saving capability of material. ΔT_{sol} is defined as the difference in the solar-energy transmittance (T_{sol}) values before and after phase transition in the 240 to 2500 nm spectrum, which is estimated using the follow equations [38]:

$$T_{sol} = \int \Phi_{sol}(\lambda)Td\lambda / \int \Phi_{sol}(\lambda)d\lambda, \ (250 \text{ to } 2600 \text{ nm})$$

$$\Delta T_{sol} = T_{sol,low\ temperature} - T_{sol,high\ temperature}$$

where Φ_{sol} denotes the solar irradiance spectrum for an air mass of 1.5, which is equivalent to the presence of the sun at an angle of 37° from the horizon [37]; moreover, $T_{sol,low\ temperature}$ and $T_{sol,high\ temperature}$ represent the solar transmittance of VO_2 films at a low temperature in the monoclinic phase and at a high temperature in the rutile phase, respectively. T_{lum} should be greater than 40% to indicate the requirement for daylight across windows, and ΔT_{sol} should be sufficiently high, at least 10%, for energy saving [39]. Furthermore, the phase-transition temperature of VO_2 (T_c = 68 °C) should be reduced from 68 °C for efficient regulation of solar energy during daytime [40]. Therefore, a reduced phase-transition temperature (T_c), high luminous transmittance (T_{lum}), and strong solar-energy modulation ability (ΔT_{sol}) are important characteristics for energy-efficient smart windows. To fulfill the demand for practical applications of energy-saving smart windows, VO_2-based thermochromic thin films should possess the following features: the phase-transition temperature (T_c) should be reduced to near-ambient temperature, and a high luminous transmittance (T_{lum} > 40%) accompanied by a strong solar-energy modulation ability (ΔT_{sol} > 10%) should be available [41,42].

Several studies have been conducted to improve the energy-saving performance of VO_2-based smart windows. For example, reductions in T_c have been achieved by doping with metal ions [43–45], or by utilizing nonstoichiometric compounds [46], strains [47], and nano-size effects [48]. Among the aforementioned methods, doping with metal ions, such as W^{6+} [49], Al^{3+} [50], Mg^{2+} [51], Sn^{4+} [52], and Mo^{6+} [53,54], is considered the most efficient. However, an increase in the dopant content results in the deterioration of phase-transition behaviors, such as a reduction in ΔT_{sol} and a broadened phase-transition temperature range [55,56]. High values of T_{lum} and ΔT_{sol} are also required to accomplish high-energy modulation efficiency for smart windows; however, these parameters involve a tradeoff, and thus, it is difficult to enhance them simultaneously [57]. Various strategies have been suggested to improve T_{lum} and ΔT_{sol} simultaneously, such as doping with Mg^{2+} [56] and F^- [55], or utilizing nano-size thermochromic materials [58], photonic crystals [59], antireflective overcoating [60], porous films [60], and multilayered structures [60,61]. However, the fabrication of VO_2(M) films with high T_{lum} (> 40%) and ΔT_{sol}(>10%) values as well as a sufficiently reduced T_c remains challenging, which limits the utilization of VO_2(M) in practical applications [56,57,62]

Recently, the fabrication of flexible VO_2(M) films has attracted widespread attention [39,56]. Flexible thermochromic films demonstrate significant potential for large-scale fabrication and commercialization [63–66]. For example, flexible VO_2(M) films can be instantly applied to the windows of existing buildings and easily integrated onto curved surfaces, such as automobile windows. Moreover, flexible VO_2(M) thin films show the potential for application in actuators and optical switches for future optical and electronic devices [63,67]. Thus far, high-quality VO_2(M) thin films have been fabricated using vacuum-chamber-based techniques, such as chemical vapor deposition (CVD) [68–70],

physical vapor deposition [56], radiofrequency (RF) magnetron sputtering [71], and pulsed laser deposition [72]. These deposition methods provide high-quality and highly crystalline VO_2(M) films; however, they often require high-temperature deposition conditions or an additional thermal annealing process to yield phase-pure crystalline VO_2(M) films [63]. The deposition temperature is typically higher than 400 °C, which exceeds the thermal resistance of most flexible polymeric substrates [51,73–75]. Therefore, chamber-based deposition processes are predominantly performed on rigid inorganic substrates with high thermal resistance, which limits the fabrication of crystalline VO_2(M) films on flexible substrates. Flexible VO_2(M) films can also be obtained via colloidal deposition using VO_2(M) nanoparticles (NPs) [56,65,76]. Colloidal dispersion of VO_2(M) enables solution-based deposition onto polymeric substrates or the formation of flexible composite films through mixing in a polymer matrix. Hydrothermal synthesis of colloidal VO_2(M) NPs was reported in a recent study, which demonstrated the feasibility of producing flexible VO_2(M) films through the solution-based deposition of NPs at room temperature [77,78]. However, for colloidal VO_2(M) NPs synthesized hydrothermally, lowering T_c while maintaining favorable optical properties, such as a high T_{lum} and ΔT_{sol}, remains difficult [79,80]. Therefore, the fabrication of flexible VO_2 thin films using colloidal VO_2(M) NPs with a reduced T_c, high T_{lum}, and high ΔT_{sol} is still significantly challenging. In this review, we focus on the recent advances in the fabrication methods for flexible thermochromic VO_2(M) thin films. We systematically review the fabrication process, including chamber-based vacuum deposition on flexible substrates that possess high thermal resistance. In addition, we introduce film-transfer techniques used to transfer VO_2(M) layers deposited on rigid substrates onto flexible polymer substrates. Finally, we introduce the solution-based deposition process using colloidal VO_2(M) NPs. The optical properties and phase transition behaviors are discussed to investigate the potential of flexible VO_2(M) films for application in energy-saving smart windows and other emerging technologies.

2. Fabrication Methods

2.1. Fabrication of Flexible Monoclinic-Phase VO_2 (VO_2(M)) Films via Chamber-Based Deposition

As discussed, the fabrication of stoichiometric and highly crystalline VO_2 films using vacuum deposition requires high-temperature conditions or an additional calcination process [81]. Therefore, rigid inorganic substrates, which have high thermal stability, such as SiO_2 [82], MgF_2 [83], and Al_2O_3 [84], are generally used for growing VO_2(M) films. The fabrication of flexible VO_2(M) films through chamber-based deposition of VO_2(M) films has also demonstrated using flexible substrates with high thermal stability. For example, muscovite sheets were first used as substrates for the fabrication of VO_2(M) films because such sheets possess a high thermal stability of over 500 °C and superior chemical resistance, which enable the formation of highly crystalline VO_2(M) films through high-temperature sintering. High-quality, single-phase VO_2(M) films can be grown epitaxially on (001) muscovite substrates with high crystallinity, leading to superior phase transition behaviors in terms of resistivity and infrared (IR) transmittance [85]. Li et al. also developed a process for depositing a VO_2 film directly on a flexible muscovite substrate [86]. First, V_2O_5 films were deposited on a native muscovite substrate through pulsed-laser deposition for 20 min; then, the films were annealed at 650 °C under a 5 mTorr oxygen atmosphere to obtain highly crystalline VO_2(M) films (Figure 2a). The electrical resistance of the VO_2(M) thin films was measured under various bending radii. During the phase transition, the electrical resistance of the films varied by an order of 10^3 or more ($\Delta R/R > 10^3$), and the change in luminous transmittance was higher than 50% ($\Delta T_r > 50\%$) (Figure 2b). Owing to the intrinsic transparency and flexibility of muscovite sheets, the VO_2/muscovite heterogeneous structures also exhibited superior flexibility and visible-light transparency. The electrical resistance of the VO_2/muscovite films remained the same even after the films were bent 1000 times; this confirmed the high mechanical stability of the films (Figure 2c). Thus, considering their enhanced electrical, thermal, optical, and mechanical

properties, VO_2/muscovite films demonstrate considerable potential for application in flexible electronic devices, especially optical switches.

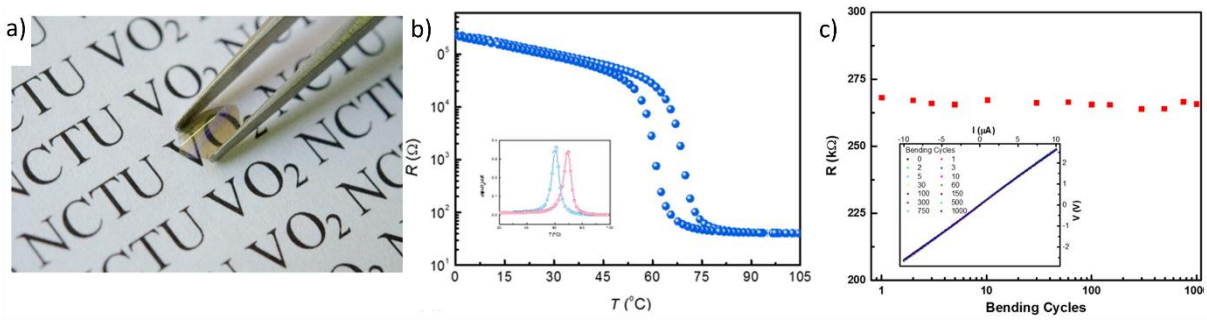

Figure 2. (**a**) Photograph of VO_2/muscovite thin film; (**b**) Temperature-dependent electrical resistance of VO_2/muscovite films; (**c**) Cyclability of VO_2/muscovite films over 1000 iterations in a bending test. Reproduced with permission from [86]. Copyright 2016, American Chemical Society.

VO_2(M) thin films grown on substrates, such as TiO_2, Al_2O_3, diamond, and SiO_2, have strong chemical bonds (ionic or covalent) between the VO_2(M) layers and the substrates. Thus, the VO_2 lattice is constrained, which is known as the substrate-clamping effect; this complicates the lattice rearrangement during phase transition [82,87,88]. Therefore, VO_2 films deposited on inorganic substrates typically require a higher energy to drive the metal–insulator transition (MIT). Conversely, VO_2(M) films deposited on mica sheets typically have weak van der Waals (vdW) bonds (0.1–10 kJ mol^{-1}) between VO_2(M) and the mica layer, which is 2–3 times weaker than the aforementioned ionic or covalent bonds (100–1000 kJ mol^{-1}) [89]. This weak vdW bonding between the VO_2 film and the mica sheet does not induce any significant lattice strain in the VO_2 layer. Therefore, the VO_2 film behaves as a nearly freestanding film on the mica sheet, which enables MIT with exceedingly low energy stimuli [90]. Moreover, owing to the weak vdW bonding between adjacent mica sheets, the thin mica sheet can be peeled off from the substrate, creating transparent and flexible VO_2(M)/mica sheets. Wang et al. also employed a mica sheet as a support for VO_2(M) to fabricate a mechanically flexible and electrically tunable flexible phase-change material for IR absorption [91]. First, 100-nm-thick Au thin films were deposited on a mica sheet through magnetron sputtering. Then, a 100-nm-thick vanadium film was deposited on the Au film via electron-beam evaporation and was thermally annealed in an oxygen atmosphere at temperatures of 430–470 °C. Au and mica sheet can withstand high-temperature annealing conditions. Finally, graphene thin films were transferred onto the VO_2 thin film to deposit the conductive electrode that induces the phase transition of the VO_2(M) thin films through Joule heating (Figure 3a). The IR absorption of this device can be continuously adjusted from 20% to 90% by changing the current applied to the graphene film. Moreover, this structure exhibited superior bending durability when it was bent up to 1500 times, without any noticeable deterioration in the optical properties (Figure 3b). Such tunable and flexible VO_2 devices have various application prospects in flexible photodetectors and active wearable devices.

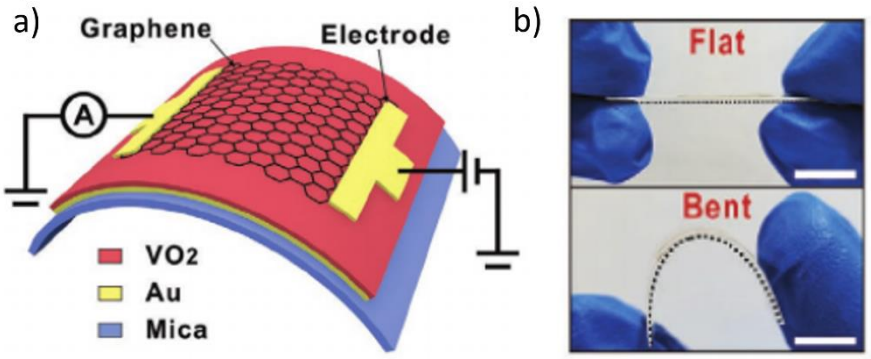

Figure 3. (**a**) Schematic representation of a flexible and electrically tuned flexible phase change material (FPCM) structure; (**b**) Mechanical flexibility of FPCM with 10 mm scale bars. Reproduced with permission from [91]. Copyright 2021, Wiley.

Chen et al. fabricated a flexible VO_2(M) thin film on a muscovite (mica) sheet directly through RF-plasma-assisted oxide molecular beam epitaxy (rf-OMBE) [92]. First, the VO_2 layer was grown using rf-OMBE on the (001) plane of mica sheets at 550 °C. Then, a layered single-walled carbon nanotube (SWNT) films was deposited using CVD on the high-quality VO_2/mica thin film. The SWNT layer exhibited superior conductivity and flexibility and can be employed as an efficient heater when a current/bias voltage is applied. The almost freestanding SWNTs/VO_2/mica (SVM) film was fabricated by peeling off the thin-layered SVM film from the substrates. Two Au electrodes were deposited on the flexible SVM thin film to provide a two-terminal electrode. The MIT process of the flexible VO_2(M) thin film can be easily controlled by heating SVM films with a bias current on Au electrodes, thereby enabling reversible modulation of IR transmission. When a bias current was applied, the transmittance decreased sharply from 70% and maintained an almost constant value of approximately 30% thereafter. When the input current was turned off, the transmittance quickly returned to its highest value of 70%; this confirms that direct modulation of the transmittance by applying a current is possible (Figure 4a,b). The MIT temperatures were 71 and 62 °C during the heating and cooling cycles, respectively (Figure 4c). Such ultrathin flexible SVM films with superior flexibility and transparency can be used for various applications involving future electrical devices.

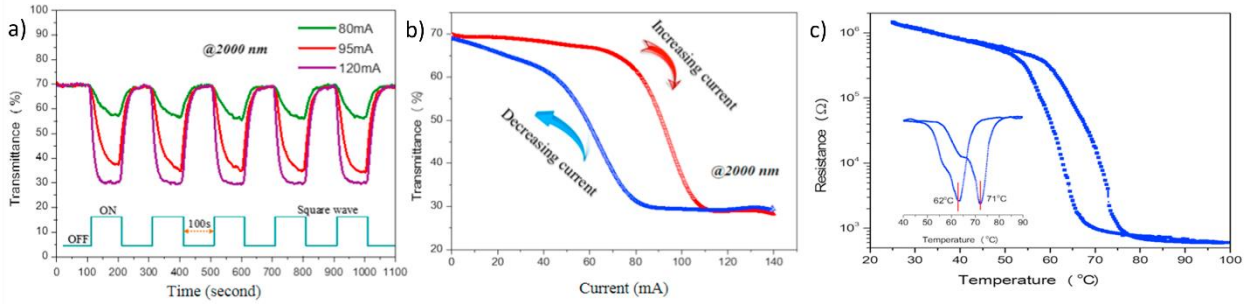

Figure 4. (**a**) Infrared (IR) response of flexible single-walled carbon nanotubes/VO_2/mica thin film with square-wave current; (**b**) IR performance as a function of applied current (2000 nm); (**c**) Resistance-dependent temperature curve for VO_2/mica thin film (the inset shows the differential curves during phase transition). Reproduced with permission from [92]. Copyright 2017, Elsevier.

In addition to mica sheets, carbon-based substrates, such as graphene sheets and networks of carbon nanotubes (CNTs), have also been utilized as flexible substrates for VO_2 deposition owing to their high thermal resistance. Xiao et al. reported the fabrication of VO_2/graphene/CNT (VGC) flexible thin films [93]. First, the graphene/CNT thin film was prepared by depositing graphene on a Cu substrate via low-pressure CVD. Then, the aligned CNT thin films were stacked on graphene substrates, followed by etching of the

Cu substrate to form flexible graphene/CNT flexible thin films. The VO_x thin film was deposited on the graphene/CNT film through DC magnetron sputtering and was then thermally annealed at 450 °C in a low-pressure oxygen environment to obtain crystalline VO_2(M) thin films (Figure 5a). The phase transition of the VGC freestanding thin film can be induced by applying a current. The VGC films exhibited fast switching with low power consumption and highly reliable phase transition (Figure 5b,c). The drastic change in IR transmittance during the phase transition can potentially enable the application of VGC films in IR thermal camouflage, cloaking, and thermal optical modulators.

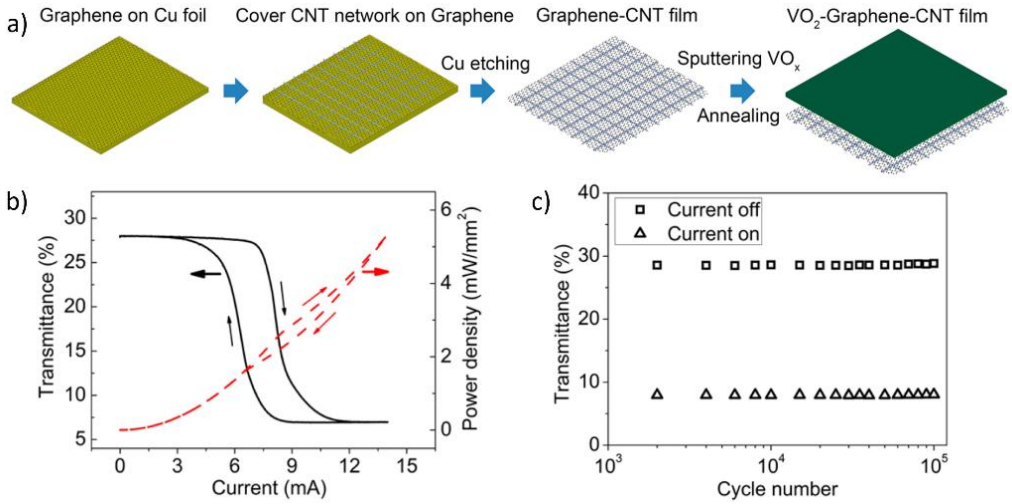

Figure 5. (**a**) Schematic of fabrication of VO_2/graphene/carbon nanotube (VGC) film; (**b**) Characterization of VGC film with current-dependent transmittance (1500 nm) (black line) and the correlated power consumption (red line); (**c**) Reliability measurement of the VGC films over 100,000 cycles with regard to current pulses. Reproduced with permission from [93]. Copyright 2015, American Chemical Society.

Chan et al. reported the fabrication of flexible VO_2(M)/Cr_2O_3/polyimide (PI) films using Cr_2O_3 as a buffer layer [94]. The Cr_2O_3 layer allows an epitaxial growth of the VO_2(M) layer, typically at approximately 300 °C, which enables the deposition of VO_2(M) on the PI polymer substrate at a relatively lower temperature (Figure 6a). The lattice constants for Cr_2O_3 are a = 0.496 nm, b = 0.496 nm, and c = 1.359 nm, and those for VO_2(R) are a = 0.455 nm, b = 0.455 nm, and c = 0.286 nm [95]. Therefore, Cr_2O_3 can act as a buffer layer owing to the similarity of its lattice constants with those of VO_2(R). Therefore, highly crystalline VO_2/Cr_2O_3 films can be successfully fabricated even under relatively low deposition conditions from 250 to 350 °C. Moreover, the refractive index of Cr_2O_3 is 2.2–2.3; hence, Cr_2O_3 behaves as an antireflective coating on top of the VO_2(M) layers, leading to a higher optical performance with T_{lum} and ΔT_{sol}. The VO_2 film fabricated at 275 °C showed 42.4% of T_{lum} and 0.4% of ΔT_{sol}; in contrast, the VO_2 film deposited with a 60-nm Cr_2O_3 buffer layer exhibits a high ΔT_{sol} value of 6.7% at a similar T_{lum} (43.7%). To fabricate flexible VO_2/Cr_2O_3/PI films, thin Cr_2O_3 layers were deposited on colorless PI films through magnetron sputtering; then, the VO_2 layers were directly deposited on Cr_2O_3/PI films using magnetron sputtering (Figure 6b). VO_2/Cr_2O_3/PI films exhibit minimal strain owing to the similar lattice parameters of the two layers. Therefore, flexible VO_2(M) films have a narrow and sharp hysteresis loop. The VO_2/Cr_2O_3/PI films exhibited superior IR modulation properties, i.e., approximately 60% variation at 2500 nm, when the VO_2 film thickness was approximately 80 nm (Figure 6c). The T_c values of the films calculated during the heating and cooling cycles were 71.8 and 71.3 °C, respectively, and the transition width of the hysteresis loop was approximately 0.5 °C, which is significantly low for a phase transition (Figure 6d,e). Furthermore, the resistivity decreased by more than two orders of magnitude during the phase transition, indicating the high crystallinity

of VO_2(M) films. However, the deposition temperature of >250 °C is still higher than the temperature that typical polymer films can withstand, which limits the utilization of various flexible polymeric substrates other than PI.

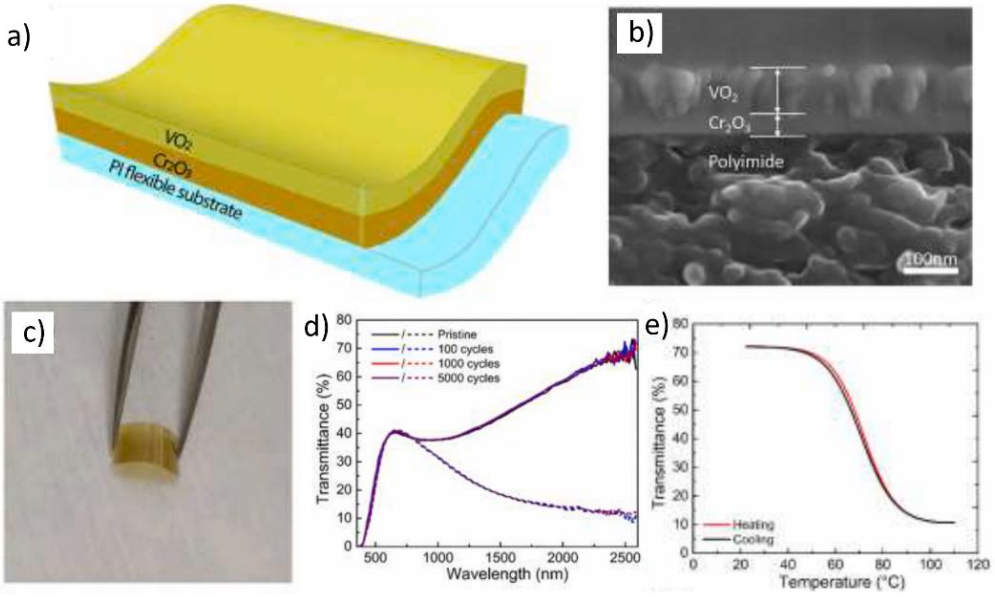

Figure 6. (**a**) Schematic representation and (**b**) cross-sectional scanning electron microscopy image of VO_2/Cr_2O_3/polyimide (PI) film; (**c**) Photograph of flexible VO_2/Cr_2O_3/PI film, (**d**) Ultraviolet–visible–near-IR (NIR) transmittance spectra of flexible VO_2/Cr_2O_3/PI film after multiple bending cycles; (**e**) Temperature-dependent transmittance hysteresis loop (2500 nm) of flexible VO_2/Cr_2O_3/PI film. Reproduced with permission from [94]. Copyright 2021, Elsevier.

Although direct deposition of VO_2(M) on substrates with high thermal resistance is a simple single-step process, only a limited number of substrates can be used under high-temperature deposition conditions. In contrast, the film-transfer process offers opportunities to utilize various types of polymeric substrates for the fabrication of flexible films [96]. In this process, VO_2(M) films are deposited on rigid substrates via high-temperature vacuum deposition and thermal annealing; then, the VO_2(M) thin films are transferred onto flexible polymeric substrates using the film-transfer process. As the VO_2(M) films are deposited under high-temperature conditions, they become highly crystalline, achieving enhanced optical properties (high T_{lum} and ΔT_{sol}) and improved stability under ambient conditions that persists for several months [97]. Moreover, polymer supports can impart enhanced mechanical stability and flexibility to films. The fabrication of flexible VO_2(M) films using the film-transfer process was first performed by Kim et al. [98]. In this process, an atomically thin, flexible graphene film was used to deposit a VO_2(M) layer for the transfer process. An amorphous VO_x layer was first deposited on a graphene/Cu substrate through RF magnetron sputtering. Then, the VO_x film on the graphene/Cu substrate was thermally annealed at 500 °C to transform VO_x into crystalline VO_2 films. The Cu substrate was selectively etched, and the remaining VO_2(M)/graphene film was transferred to a polyethylene terephthalate (PET) film to fabricate flexible VO_2(M)/graphene/PET films. Because of the deposition on polymer films, the VO_2(M)/graphene/PET films exhibited high mechanical stability and flexibility while maintaining their reversible phase-transition property. These flexible VO_2/graphene/PET films exhibited a transmittance of 65.4% at a 550-nm wavelength; moreover, the variation in the transmittance during phase transition reached 53% at a wavelength of 2500 nm, with the transition band width being 9.8 °C (Figure 7a,b). The VO_2(M)/graphene/PET was integrated onto glass in a model house to investigate its ability to regulate the indoor temperature when functioning as a smart window. The VO_2/graphene films reduced the indoor room temperature by 5.8 °C compared

with bare glass, thereby exhibiting the potential to function as an energy-efficient smart window (Figure 7c,d).

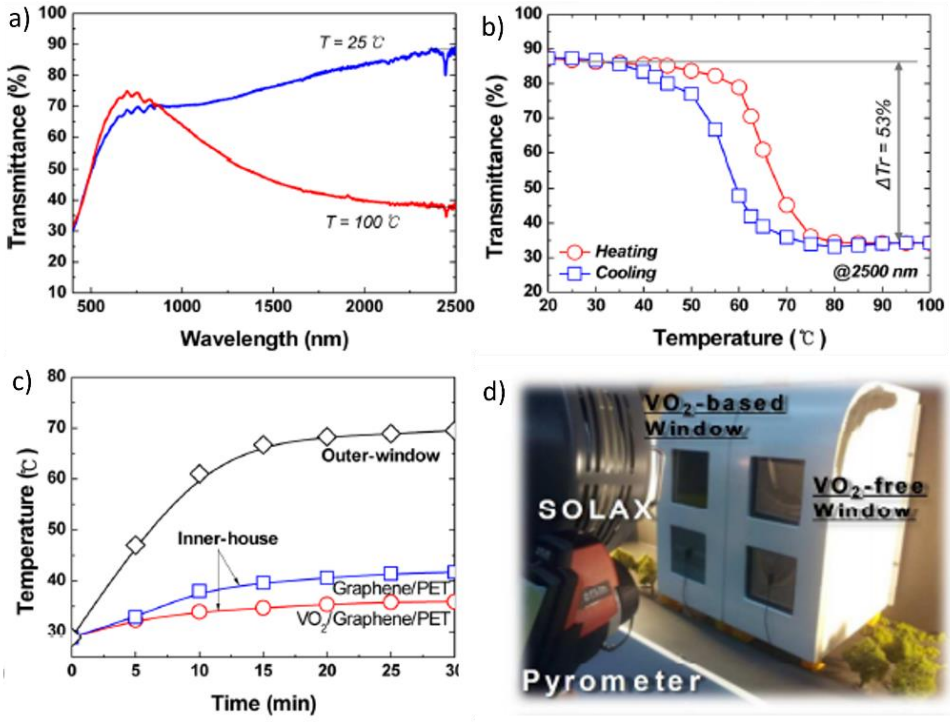

Figure 7. (**a**) Transmission spectra of VO_2/graphene/polyethylene terephthalate (PET) film at 25 and 100 °C; (**b**) Temperature-dependent transmittance of VO_2/graphene/PET film at 2500 nm; (**c**) Indoor temperature of a model house with VO_2/graphene/PET films; (**d**) Photograph of a model house coated with VO_2/graphene/PET films (VO_2-based windows) and graphene/PET films (VO_2-free windows). Reproduced with permission from [98]. Copyright 2013, American Chemical Society.

The fabrication of flexible VO_2(M) thin films with a reduced T_c is still challenging owing to the difficulty in doping during the deposition process. Chae et al. reported a solution-based process to deposit VO_2(M) films using W-doped colloidal NPs, followed by film transfer, to fabricate flexible W-doped VO_2(M) films [74]. Colloidal VO_x NPs were synthesized via high-temperature thermal decomposition with vanadium precursors, which were used for the deposition of VO_2(M) layers [99]. During the synthesis, W precursors were added into the reaction mixture for efficient doping of W during the formation of VO_x NPs. Then, VO_x NPs were deposited on mica substrates using the solution-based process and thermally annealed to form highly crystalline VO_2(M) films. Subsequently, the VO_2(M)/mica films were transferred onto polymeric substrates using adhesive-coated PET films. During the transfer process, a thin layer of mica sheet was peeled off and transferred to the polymer film to form transparent and flexible mica/VO_2(M)/PET films. As mica sheets are brittle, the polymer substrate can provide high mechanical strength and ensure reliable bending (Figure 8a). The W dopants were effectively doped into the VO_2(M) thin films, which resulted in the systematic reduction in T_c depending on the different possible doping concentrations. The T_c of flexible mica/VO_2(M)/PET films can be easily controlled at 25.6 °C when 1 at% W doping is used (Figure 8b). These flexible films exhibit superior optical properties—a T_{lum} of 53% and a ΔT_{sol} of 10%—at a T_c of 29 °C when 1.3 at% Tungsten (W) doping is used. Thus, such films can be viable for use in energy-saving smart windows (Figure 8c,d).

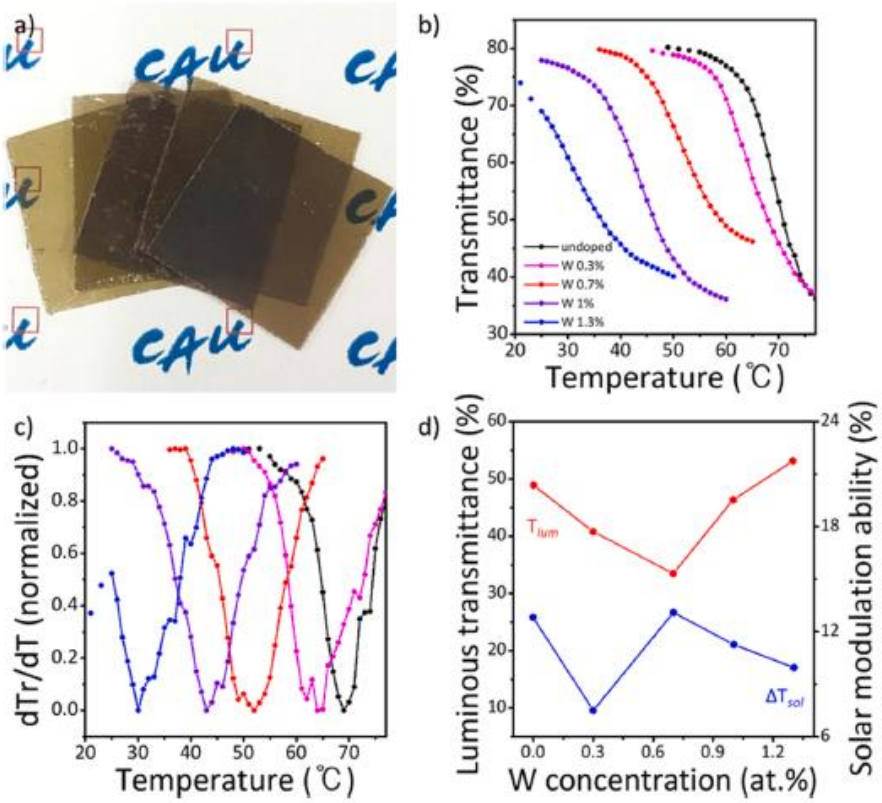

Figure 8. (**a**) Photograph of VO_2(M) thin films on PET substrates for various W doping concentrations; (**b**) Temperature dependence of transmittance; (**c**) First derivatives of transmittance; (**d**) Luminous transmittance (T_{lum}) and solar modulation ability (ΔT_{sol}) of VO_2(M)/mica thin films under various W doping concentrations (1900 nm). Reproduced with permission from [74]. Copyright 2021, Elsevier.

2.2. Fabrication of Flexible VO_2(M) Films through Solution-Based Deposition Process

Although the vacuum chamber-based deposition and film-transfer processes are highly effective for the fabrication of crystalline VO_2(M) films on flexible substrates, these processes are significantly complex, involving multiple deposition steps and often requiring an etching process, which can potentially limit large-scale fabrication and commercialization [100]. In contrast, the solution-based process enables simple, low-cost, and large-area fabrication of flexible VO_2(M) films [101]. Early examples of solution-processed VO_2(M) films were demonstrated via a sol–gel process [102]. Speck et al. were the first to demonstrate the sol–gel deposition of VO_2(M) films using molecular vanadium precursors [103]. In general, the sol–gel process of VO_2(M) thin films have been performed on thermally stable substrates, such as quartz, mica, or silicon wafers, owing to the high temperature thermal annealing process, typically above 400 °C [104]. Recent literature demonstrates that low temperature sol–gel deposition of VO_2(M) film processes can be achieved using deep ultraviolet photoactivation chemistry, which enable the fabrication of flexible VO_2(M)/Al_2O_3/PI films at 250 °C [105]. Not only has the sol–gel process been widely studied for the fabrication of flexible smart windows, but solution-based deposition using colloidal VO_2(M) NPs has too. Among a variety of synthetic methods based on colloidal VO_2(M) NPs, hydrothermal synthesis has attracted considerable attention owing to the high phase purity of the as-synthesized VO_2(M) NPs [38]. Hydrothermal synthesis involves a chemical reaction that yields high-quality crystals in a sealed pressurized reactor under high pressure and temperature. Hydrothermal growth of VO_2(M) films on the substrates has also been reported in the literature [106,107]. For example, VO_2(M) films have been fabricated via hydrothermal reactions by placing r-Al_2O_3 substrates in a hydrothermal reactor containing a solution mixture of ammonium metavanadate and oxalic acid [108]. The self-organized VO_2(M) films were formed with T_{lum} of 65% and ΔT_{sol}

of ~11.82% [109]. However, for the direct hydrothermal deposition of VO_2(M) films on flexible substrates, the substrates should have high thermal and chemical resistance to ensure that they can withstand hydrothermal reaction conditions and calcination temperature [110–112]. Therefore, the use of VO_2(M) NPs for film depositions could have potential for large-area fabrication by mass-production processes using various substrate types. The single-step hydrothermal synthesis of VO_2(M) NPs was first demonstrated by Théobald et al. using a V_2O_3–V_2O_5–H_2O system, and the reaction was performed at a temperature of 20–400 °C under supercritical pressure [113]. There exist several stable vanadium oxide structures, such as VO_2, V_2O_5, V_2O_3, V_5O_9, V_6O_{13}, and V_6O_{11}, with various nonstoichiometric compounds [114]. Even in the stoichiometric compound, i.e., VO_2, several polymorphs exist, such as VO_2(A) [115], VO_2(B) [59], VO_2(D) [116], VO_2(P) [117], and VO_2(M) [118]. Therefore, hydrothermal synthesis of phase-pure and highly crystalline VO_2(M) is significantly challenging. Strong phase transition behaviors and favorable optical properties, including high values of T_{lum} and ΔT_{sol}, can be obtained using high-purity VO_2(M) NPs, in the absence of nonstoichiometry and impurities of metastable polymorphs. Therefore, careful control of synthetic procedures, including the hydrothermal reaction conditions, types of metal precursors, solvents, and additives, is a prerequisite for obtaining phase-pure VO_2(M) NPs.

To enhance phase purity and crystallinity, a two-step hydrothermal synthesis process to synthesize VO_2(M) NPs has widely studied. In this process, metastable VO_2 NPs are first synthesized hydrothermally and then thermally annealed for the conversion into the VO_2(M) phase. Phase-pure VO_2(M) NPs are obtained from various types of metastable VO_2 NPs and under different annealing conditions. Xie et al. first reported the hydrothermal synthesis of VO_2(D) with a size of 1–2 μm, using NH_4VO_3 and $H_2C_2O_4$. Hydrothermal synthesis was performed at 210 °C for 24 h, followed by a calcination process to transform the VO_2(D) into VO_2(M) [116]. Calcination of VO_2(D) was performed at temperatures as low as 300 °C for 2 h under a flow of high-purity nitrogen to obtain VO_2(R) NPs. These NPs also exhibit MIT near 68 °C. A two-step hydrothermal synthesis using VO_2(B) NPs has also been reported; however, the phase transformation from VO_2(B) to VO_2(M) occurs at a significantly higher annealing temperature, typically higher than 500 °C [119]. Corr et al. also studied the hydrothermal synthesis of VO_2(B) nanorods using V_2O_5 and formaldehyde solution at 180 °C for two days [120]. Then, thermal annealing was performed to convert VO_2(B) to VO_2(R) at 700 °C for 1 h in an argon atmosphere. Sun et al. reported the hydrothermal synthesis of VO_2(P) using $VO(OC_3H_7)_3$ and oleylamine at 220 °C for 48 h; then, they obtained VO_2(M) after thermal annealing at 400 °C for 40 or 60 s in a nitrogen or air atmosphere [121]. The size-dependent MIT property of VO_2(M) NPs was demonstrated through in situ variable-temperature IR spectroscopy. The authors observed that the variation in the transmittance of single-domain VO_2(M) NPs during phase transition systematically increased with a reduction in the size of the VO_2(M) NPs. Zhong et al. reported star-shaped VO_2(M) NPs that were hydrothermally synthesized using NH_4VO_3 and formic acid for two days at 200 °C. Then, the as-synthesized NPs were thermally annealed at 300–450 °C for 1 h to obtain VO_2(M) NPs. The VO_2(M) NP thin films were 325 nm thick and exhibited a T_{lum} and ΔT_{sol} of 44.18% and 7.32%, respectively [122]. Song et al. reported the hydrothermal synthesis of VO_2(D) using NH_4VO_3 and $H_2C_2O_4{\cdot}2H_2O$ at ~220 °C for ~18 h, followed by thermal annealing of VO_2(D) at 250–600 °C for 3 h, to obtain VO_2(M) nanoaggregates [123]. The as-synthesized VO_2(M) exhibited a low T_c of approximately 41.0 °C and a thermal hysteresis width of approximately 6.6 °C. Li et al. demonstrated the electrothermochromicity of VO_2(M) NPs/Ag nanowire (NW) thin films deposited on glass and flexible PET substrates [124]. VO_2(M) NPs were hydrothermally synthesized using V_2O_5 and an oxalic acid dehydrate via at 220 °C for 36 h, followed by additional thermal annealing at 400 °C for 1 h in a vacuum chamber. The VO_2(M) NPs were deposited on top of Ag NW heaters. The optical response of the VO_2(M) NP films was then dynamically modulated by applying voltage on Ag NW. The infrared (IR) transmittance variation of the films from 0 V to 8 V of applied voltage is approximately 50%

at 1500 nm. Li et al. demonstrated the two-step hydrothermal synthesis of VO_2(M) NPs using V_2O_5, $H_2C_2O_4$, and polyvinyl alcohol precursors [125]. The hydrothermal synthesis was performed at 220 °C for over 36 h, and the calcination was performed at 300–450 °C under vacuum. The VO_2(M) film had a thickness of 463 nm and exhibited a high T_{lum} of over 70% at 700 nm; moreover, its IR transmittances at 1500 nm were approximately 89.5% and 53.8% before and after phase transition, respectively. The IR modulation exceeded 35%, which represents favorable optical properties for application in smart windows.

A single-step hydrothermal synthesis without a calcination process has also been reported. This method is a potentially simple, convenient, and low-cost process because it involves no additional post-annealing to obtain phase-pure VO_2(M) NPs [126]. An additional thermal annealing processes induces grain growth in VO_2(M) films. Size dependence of VO_2(M) NPs on thermochromic properties have also been reported. Notably, a decrease in the size of VO_2(M) NPs improves T_{lum} and ΔT_{sol} values [80]. Narayan et al. reported a phase-transition model in which the hysteresis width is directly proportional to the grain boundary area per unit volume [127]. Therefore, the hysteresis width is inversely correlated to the particle radius, and as the particle size increases, the phase transition temperature reduces, and the hysteresis width decreases. The smaller the nanoparticle size, the wider the hysteresis, and the VO_2 thermochromic performance is improved [128,129]. Therefore, single-step hydrothermal synthesis is more preferable to prevent particle coarsening by an additional thermal annealing process, hence sustaining a high thermochromic performance [130,131]. Gao et al. first demonstrated single-step hydrothermal synthesis of W-doped snowflake-shaped VO_2(R) using V_2O_5 and $H_2C_2O_4$. The reaction was performed for seven days at 240 °C, and VO_2(M) NPs were synthesized without a thermal annealing step [78]. The width of the VO_2(R) nanocomposites was 200–300 nm, and the thickness was approximately 200–800 nm. Alie et al. also demonstrated single-step hydrothermal synthesis of star-shaped and spherical VO_2(M) particles using $H_2C_2O_4$ and V_2O_5 in a molar ratio of 3:1 at 260 °C for 24 h [132]. The highly crystalline star-shaped VO_2(M) particles exhibited a high thermal stability of up to ~300 °C and a >10% transmittance variation in the IR region during phase transition. Li et al. reported one-step hydrothermal synthesis of VO_2(M) NPs using V_2O_5, TiO_2, and $H_2C_2O_4 \cdot 2H_2O$ at 240 °C for 24 h [133]. The VO_2(M) NPs, with a size of approximately 50–100 nm, were further modified using $Zn(CH_3COO)_2$ to obtain a VO_2–ZnO structure. The VO_2(M)–ZnO films exhibited a low T_c of approximately 62.6 °C and a T_{lum} and ΔT_{sol} of approximately 52.2% and 9.3%, respectively. Ji et al. demonstrated the synthesis of VO_2(M) using V_2O_5, N_2H_4, and H_2O_2 through a one-step hydrothermal process performed at 260 °C for 24 h (Figure 9a,b). The as-prepared VO_2(M) NPs exhibited a transmittance change of approximately 50% at a wavelength of 2000 nm [134]. Moreover, as the concentration of the W dopant increased from 0% to 1%, the T_c of the VO_2(M) NPs decreased from 55.5 to 37.1 °C (Figure 9c). Chen et al. reported the synthesis of phase-pure $V_{1-x}W_xO_2$ nanorods using $H_2C_2O_4 \cdot 2H_2O$ and V_2O_5 precursors. For W doping, $(NH_4)_5H_5[H_2(WO_4)_6]H_2O$ was added, and the reaction was performed at 260–280 °C for 6–72 h [135]. The T_{lum} of the 0.5 at% W-doped VO_2(M) films was 60.6% at 20 °C, and ΔT_{sol} was 8.1%. Whittaker et al. reported the synthesis of W-doped VO_2(M) nanobelts using V_2O_5 and $H_2C_2O_4$ precursors with H_2WO_4 for W doping [43]. The reaction was performed at 250 °C for 12 h to 7 days. W doping (0.90%) led to remarkable modulation of the T_c of VO_2(M) films, from 68.0 to 33.8 °C. Shen et al. demonstrated that Zr doping significantly enhances optical properties while reducing T_c. [118]. Moreover, Zr doping of VO_2(M) reduces T_c while improving T_{lum} and ΔT_{sol}. However, T_c is only reduced from 68.6 to 64.3 °C with 9.8% Zr doping; conversely, Zr-doped VO_2 flexible films exhibit high values of T_{lum} (60.4%) and T_{sol} (14.1%). The optical bandgap, which is 1.59 eV for undoped VO_2(M), increases to 1.89 eV after 9.8% Zr doping, resulting in a change in the apparent color of the VO_2(M) films. Accordingly, the color of the Zr-doped VO_2(M) flexible films is affected; the brown-yellow color of flexible VO_2(M) film is brightened, along with an increase in T_{lum}. In addition, T_c is further reduced to 28.6 °C, and T_{lum} and ΔT_{sol} values of 48.6% and 4.9%, respectively, are achieved through W-Zr-co-doping.

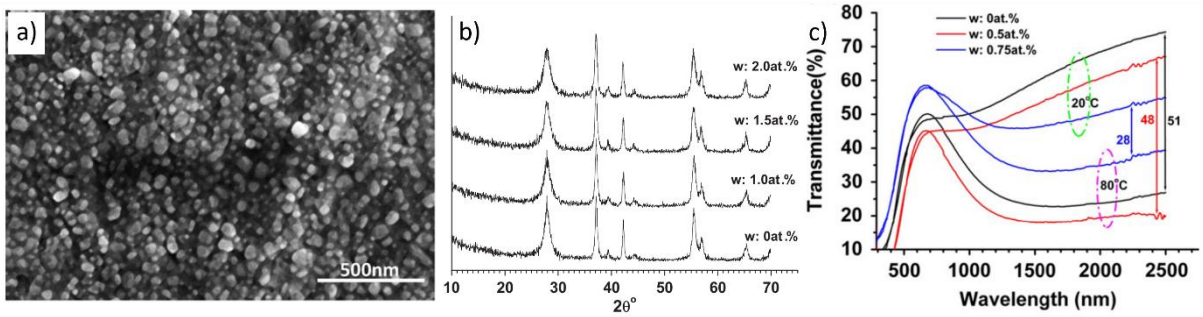

Figure 9. (**a**) SEM image and (**b**) XRD patterns of VO_2(M) NPs; (**c**) Temperature-dependent transmittance spectra during phase transition of VO_2(M) film. Reproduced with permission from [134]. Copyright 2011, Elsevier.

Several studies have been conducted to optimize the conditions for single-step hydrothermal synthesis to enhance the phase purity of VO_2(M) NPs and their optical properties, including T_{lum} and ΔT_{sol}. Guo et al. performed a one-step hydrothermal synthesis process using $VOSO_4$ and $N_2H_4 \cdot H_2O$ in the presence of H_2O_2 [77]. H_2O_2, a strong oxidizing agent, is separated after the reaction with the vanadium solution in a hydrothermal autoclave reactor. Then, H_2O_2 decomposes and evaporates at 150 °C to provide a moderately oxidizing environment. This facilitates the synthesis of stoichiometric and highly crystalline VO_2(M) NPs. The as-synthesized VO_2(M) NPs exhibited an average size of ~30 nm, with significant size uniformity (Figure 10a,b). For the preparation of flexible VO_2(M) films, the VO_2(M) NPs were dispersed in N,N-dimethylformamide with polyacrylonitrile polymers. Then, the solution was deposited on a flexible PET substrate. The flexible VO_2(M) films attained favorable optical properties, with a T_{lum} of 54.26% and a ΔT_{sol} of 12.34% (Figure 10c,d). In addition to optimizing the hydrothermal reaction conditions, the enhancement in the purity of vanadium precursors also produces VO_2(M) NPs with improved optical properties.

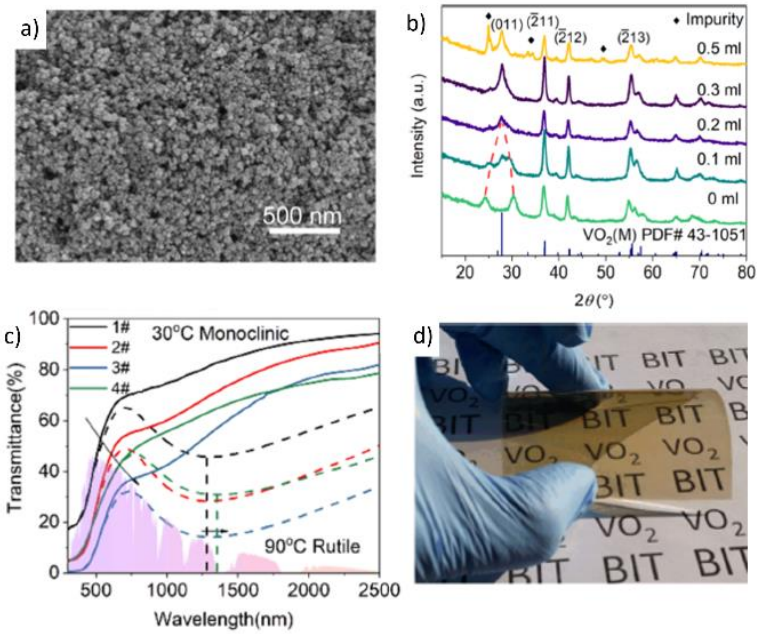

Figure 10. (**a**) SEM image of the VO_2 NPs with 0.2 mL of H_2O_2, (**b**) XRD patterns of as-synthesis VO_2 NPs with different amounts of H_2O_2, (**c**) temperature-dependent transmittance spectra of samples at 30 °C (bold line) and 90 °C (dashed line), and (**d**) the VO_2(M) NPs-based flexible films. Reproduced with permission from [77]. Copyright 2018, American Chemical Society.

Kim et al. demonstrated single-step hydrothermal synthesis of VO_2(M) NPs using phase-pure vanadium precursors [136]. After mixing the vanadium precursors, size-

selective purification was performed to enhance the phase purity of the precursors, resulting in the formation of VO_2(M) NPs with enhanced optical properties. The obtained phase-pure VO_2(M) NPs exhibited an enhanced T_{lum} (55%) and ΔT_{sol} (18%), and the ΔT_{sol} value is one of the highest reported for hydrothermally synthesized VO_2(M). Furthermore, W-doped VO_2(M) NPs have been reported to exhibit superior phase-transition behaviors, while T_c is systematically reduced depending on the W doping concentration (Figure 11a,b). Flexible VO_2(M) films were fabricated and deposited on PET polymer substrates over a large area using a spray coater (15 cm × 15 cm) (Figure 11c,d). In model house experiments under daytime solar irradiation, the W-doped VO_2(M) films applied onto glass provided a significant reduction in the indoor temperature; thus, these films are potentially viable for practical applications.

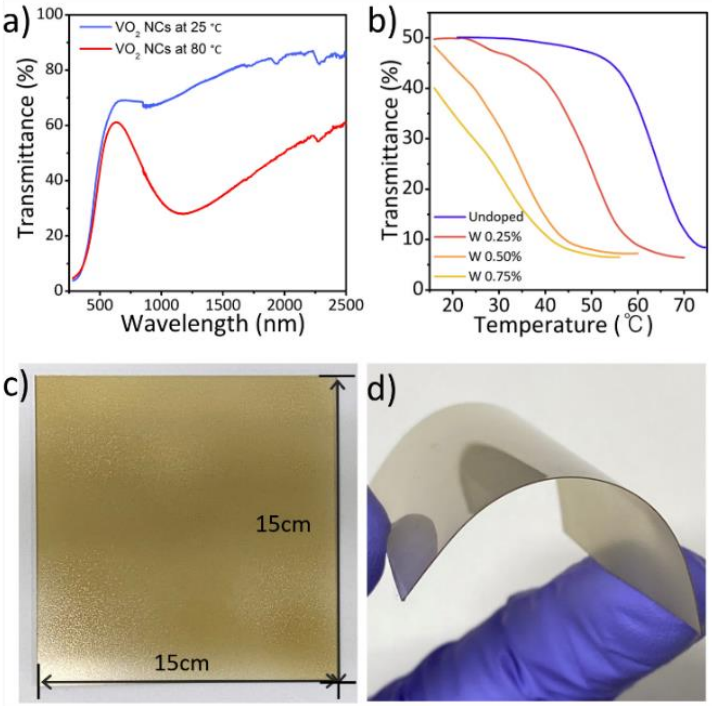

Figure 11. (**a**) Transmittance spectra of VO_2(M) NP films before and after phase transition; (**b**) Temperature-dependent transmittance (1350 nm) of W-doped VO_2(M) NP films during heating; Photographs of (**c**) 15 cm × 15 cm VO_2(M) NP films on glass substrate and (**d**) flexible substrate obtained via spray-coating. Reproduced with permission from [136]. Copyright 2021, Elsevier.

Colloidal NPs enable convenient, large-scale fabrication of flexible VO_2(M) film through the solution process, which is beneficial considering the expected requirement for large-scale fabrication techniques [63,65,76,137]. For the fabrication of flexible VO_2(M) films, VO_2(M) NPs have been coated on flexible polymer films or embedded into a polymer matrix [138]. Shen et al. reported a process for blade coating of VO_2(M) NPs on indium tin oxide (ITO)-coated PET substrates to form flexible VO_2(M) films [139]. Applying a current along the ITO layer induced ohmic heating, which resulted in the phase transition of VO_2(M) layers and a change in IR transmittance. The obtained film showed well-controlled IR switching properties upon changing the input voltage, as well as superior thermochromic properties (T_{lum} of 57.3% and ΔT_{sol} of 13.8%). Under ohmic heating, the IR conversion properties did not show any evident deterioration, even after 10,000 bending cycles, which indicates superior stability and flexibility. Chen et al. demonstrated the preparation of VO_2(M)/polymer composite films by embedding VO_2(M) NPs into a polymeric matrix. VO_2(M) NPs were synthesized hydrothermally using V_2O_5 and N_2H_4 at approximately 180–400 °C for 15 h [80]. The size of the VO_2(M) NPs ranged from approximately 25 to 45 nm. The synthesized VO_2(M) NPs were dispersed in polyurethane

(PU) and coated onto PET to form flexible VO_2(M) films. These films achieved high optical performance, with a ΔT_{sol} of 22.3% and a T_{lum} of 45.6%. Similarly, Zhou et al. reported the roll-coating of Mg-doped VO_2(M) NPs that were hydrothermally synthesized using V_2O_5 and $H_2C_2O_4$ [140]. Mg-doped VO_2(M) composite foils were prepared by mixing NPs with PU solutions and were deposited on a PET substrate using a roll-coater. The flexible composite foils exhibited a high T_{lum} and ΔT_{sol} of 54.2% and 10.6%, respectively. Liang et al. reported the bar-coating of W-doped VO_2(M) nanorods; the nanorods were prepared via one-step hydrothermal synthesis for 48 h at 240 °C using V_2O_5, $C_4H_6O_6$, and ammonium tungstate (Figure 12a,b) [49]. The nanorods were then mixed with the tetraethyl orthosilicate and poly(ethyl methacrylate) solution. The solution mixture was cast on PET substrates using a stainless-steel coating bar to fabricate large-area, flexible VO_2(M) films (Figure 12c). The T_c of the flexible VO_2(M) films could be systematically modulated by approximately 24.52 °C for 1 at% of W doping, and the mid-infrared transmission could be modulated by 31% at a T_c of 37.3 °C. Inkjet printing has also been widely utilized as a useful direct-write technology to fabricate high-resolution, low-cost, large-area, and uniform-surface films on flexible substrates [141,142]. Haining et al. reported the fabrication of VO_2(M) smart windows via inkjet printing using hydrothermally synthesized VO_2(M) NPs [143,144]. Large-area VO_2(M) films were fabricated on polyethylene substrates with a T_{lum} of 56.96% and a ΔT_{sol} of 5.21%.

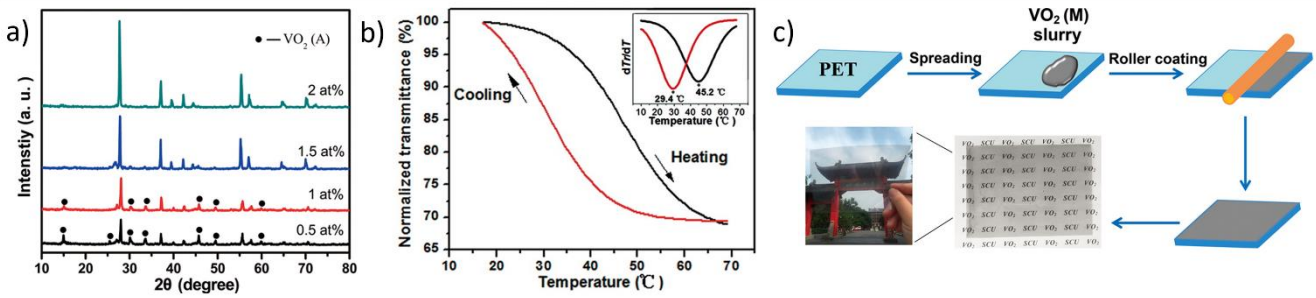

Figure 12. (**a**) XRD patterns of W doped VO_2(M) films, (**b**) Transmittance hysteresis loops and first derivatives of transmittance for W doped VO_2 (M) films recorded at a wavelength of 9 μm, (**c**) Schematic diagram of film deposition with W doped VO_2(M) NPs on PET substrates. Reproduced with permission from [49]. Copyright 2016, American Chemical Society.

The chemical instability of VO_2(M) NPs can potentially limit their long-term usage as smart windows in real-world environments [145]. To enhance the chemical stability of VO_2(M) NPs, core–shell structures, in which VO_2(M) NPs are overcoated with chemically inert shells, have been developed. Gao et al. reported a core–shell structure with VO_2@SiO_2 NPs. VO_2(M) was synthesized through a hydrothermal reaction, and SiO_2 shells were overcoated using the Stöber method [56]. SiO_2 is chemically inert and optically transparent, which is ideal for protecting VO_2(M) NPs. VO_2@SiO_2 NPs exhibit improved chemical resistance to oxidation. The SiO_2 shell of VO_2 NPs serves as an oxygen diffusion barrier layer, which can prevent the VO_2 from changing to V_2O_5. This phenomenon was confirmed through experiments conducted with VO_2 NPs and VO_2@SiO_2 NPs after annealing in an air atmosphere for 2 h at 300 °C. Flexible films were fabricated by embedding VO_2@SiO_2 NPs into a PU matrix; then, the VO_2@SiO_2 NPs/PU cast on a PET matrix were dispersed to fabricate flexible VO_2@SiO_2/PU composite films. These films exhibited a high T_{lum} (55.3%) and ΔT_{sol} (7.5%). In addition to SiO_2, various types of oxides, such as ZnS [146], TiO_2 [11], and ZrO_2 [147], have been utilized for overcoating to prepare core–shell NPs. Saini et al. demonstrated an approach to improve the thermal stability and thermochromic properties of VO_2(M) NPs by overcoating with CeO_2 [148]. VO_2(M)@CeO_2 NPs were observed to be thermally stable for up to 320 °C in air, which confirmed the enhancement in stability after overcoating.

3. Perspectives

Flexible VO_2(M) films offer significant potential for the integration of energy-saving smart windows in existing buildings, as well as for application in novel flexile devices, such as sensors and actuators. Various methods for fabricating flexible thermochromic thin films based on the vacuum deposition and solution-based process have been reported; these methods are potentially suitable for commercialization. However, certain issues still remain to be resolved before VO_2-based smart windows can be utilized in practice. For example, flexible VO_2 films fabricated using vacuum deposition and film-transfer techniques show high T_{lum} and ΔT_{sol} values; however, these methods are still limited in terms of large-area and mass-production capabilities. In addition, deposition methods with uniform doping should be developed further to systematically reduce T_c while maintaining favorable phase-change optical properties. Conversely, the annealing-free, solution-based process offers advantages such as convenient, low-cost, large-area deposition of phase-change VO_2(M) on flexible substrates. Particularly, hydrothermal synthesis yields highly crystalline VO_2(M) NPs with colloidal stability and moderately useful phase-change behaviors. However, it is still challenging to prepare flexible VO_2(M) films with high T_{lum} and ΔT_{sol} values as well as a reduced T_c. The optical properties of the representative flexible VO_2 films fabricated using deposition and solution-based processes are summarized in Figure 13, which displays the opportunities for utilizing flexible VO_2(M) films in energy-saving smart windows. Therefore, large-scale, high-throughput, mass-production capabilities for the fabrication and commercialization of high-performance VO_2(M) films should be realized. Finally, certain limitations in terms of the intrinsic properties of VO_2(M) should be overcome to utilize flexible VO_2 films. First, phase-change VO_2 films show an inherent brown color, which is not desirable for window applications. Therefore, it is highly recommended to develop fabrication methods that can enable control of the apparent colors of VO_2(M) while ensuring a high T_{lum} and ΔT_{sol} and low T_c. Moreover, vanadium oxide has various stable phases and a stable stoichiometry; consequently, VO_2(M) films are easily oxidized into other phases under exposure in ambient conditions. Therefore, processes to prevent VO_2(M) from being oxidized, for example, overcoating of VO_2(M) films or using NPs with protective layers, should be developed to enable long-term usage of the films.

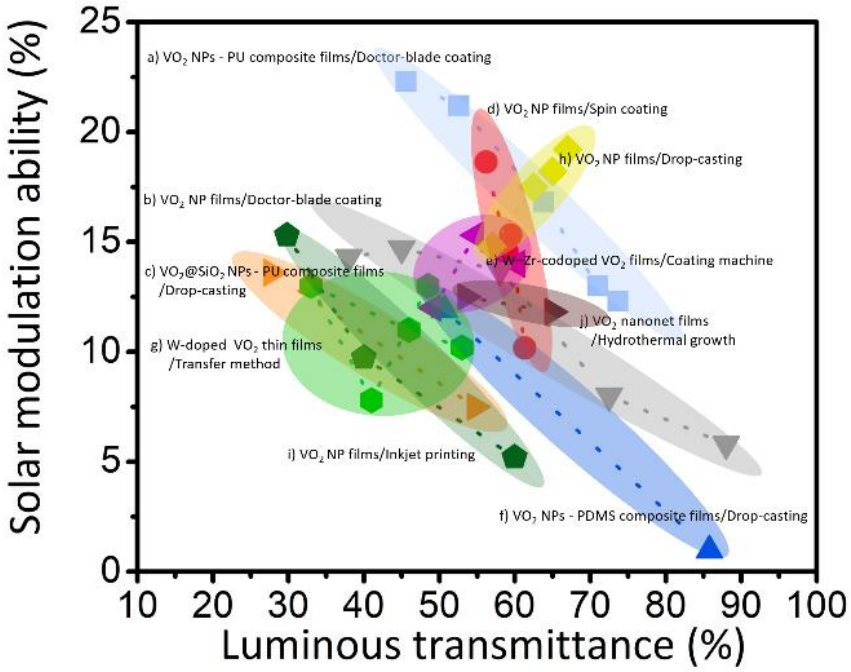

Figure 13. Comparison of luminous transmittance (T_{lum}) and solar modulation ability (ΔT_{sol}) between flexible VO_2 thin films fabricated via hydrothermal reaction: (a) [80], (b) [139], (c) [56], (d) [136], (e) [118], (f) [149], (g) [74], (h), [64], (i) [143], (j) [109].

Author Contributions: The manuscript was written through equal contributions from all authors. Investigation, J.K. and T.P.; writing—review and editing, J.K. and T.P.; supervision, T.P.; funding acquisition, T.P. All authors have read and agreed to the published version of the manuscript.

Funding: This research was supported by Creative Materials Discovery Program through the National Research Foundation of Korea (NRF) funded by the Ministry of Science and ICT (NRF-2018M3D1A1059001) and by the National Research Foundation of Korea (NRF) grant funded by the Korea government (MSIT) (NRF-2021R1A2C1013604). This research was also supported by the Chung-Ang University Graduate Research Scholarship in 2020.

Institutional Review Board Statement: Not applicable.

Informed Consent Statement: Not applicable.

Data Availability Statement: The data presented in this study are available on request from the corresponding author.

Conflicts of Interest: The authors declare no conflict of interest.

References

1. Gao, Y.; Luo, H.; Zhang, Z.; Kang, L.; Chen, Z.; Du, J.; Kanehira, M.; Cao, C. Nanoceramic VO2 thermochromic smart glass: A review on progress in solution processing. *Nano Energy* **2012**, *1*, 221–246. [CrossRef]
2. Granqvist, C.G. Transparent conductors as solar energy materials: A panoramic review. *Sol. Energy Mater. Sol. Cells* **2007**, *91*, 1529–1598. [CrossRef]
3. Ke, Y.; Zhou, C.; Zhou, Y.; Wang, S.; Chan, S.H.; Long, Y. Emerging thermal-responsive materials and integrated techniques targeting the energy-efficient smart window application. *Adv. Funct. Mater.* **2018**, *28*, 1800113. [CrossRef]
4. Chao, D.; Zhu, C.; Xia, X.; Liu, J.; Zhang, X.; Wang, J.; Liang, P.; Lin, J.; Zhang, H.; Shen, Z.X. Graphene quantum dots coated VO_2 arrays for highly durable electrodes for Li and Na ion batteries. *Nano Lett.* **2015**, *15*, 565–573. [CrossRef] [PubMed]
5. Morin, F. Oxides which show a metal-to-insulator transition at the Neel temperature. *Phys. Rev. Lett.* **1959**, *3*, 34. [CrossRef]
6. Tripathi, A.; John, J.; Kruk, S.; Zhang, Z.; Nguyen, H.S.; Berguiga, L.; Romeo, P.R.; Orobtchouk, R.; Ramanathan, S.; Kivshar, Y. Tunable Mie-Resonant Dielectric Metasurfaces Based on VO_2 Phase-Transition Materials. *ACS Photonics* **2021**, *8*, 1206–1213. [CrossRef]
7. Jorgenson, G.; Lee, J. Doped vanadium oxide for optical switching films. *Sol. Energy Mater.* **1986**, *14*, 205–214. [CrossRef]
8. Budai, J.D.; Hong, J.; Manley, M.E.; Specht, E.D.; Li, C.W.; Tischler, J.Z.; Abernathy, D.L.; Said, A.H.; Leu, B.M.; Boatner, L.A. Metallization of vanadium dioxide driven by large phonon entropy. *Nature* **2014**, *515*, 535–539. [CrossRef]
9. Aetukuri, N.B.; Gray, A.X.; Drouard, M.; Cossale, M.; Gao, L.; Reid, A.H.; Kukreja, R.; Ohldag, H.; Jenkins, C.A.; Arenholz, E. Control of the metal–insulator transition in vanadium dioxide by modifying orbital occupancy. *Nat. Phys.* **2013**, *9*, 661–666. [CrossRef]
10. Wu, C.; Feng, F.; Xie, Y. Design of vanadium oxide structures with controllable electrical properties for energy applications. *Chem Soc Rev* **2013**, *42*, 5157–5183. [CrossRef]
11. Li, Y.; Ji, S.; Gao, Y.; Luo, H.; Kanehira, M. Core-shell VO_2@TiO_2 nanorods that combine thermochromic and photocatalytic properties for application as energy-saving smart coatings. *Sci. Rep.* **2013**, *3*, 1–13. [CrossRef]
12. Goodenough, J.B. The two components of the crystallographic transition in VO_2. *J. Solid State Chem.* **1971**, *3*, 490–500. [CrossRef]
13. Whittaker, L.; Patridge, C.J.; Banerjee, S. Microscopic and nanoscale perspective of the metal− insulator phase transitions of VO_2: Some new twists to an old tale. *J. Phys. Chem. Lett.* **2011**, *2*, 745–758. [CrossRef]
14. Wu, B.; Zimmers, A.; Aubin, H.; Ghosh, R.; Liu, Y.; Lopez, R. Electric-field-driven phase transition in vanadium dioxide. *Phys. Rev. B* **2011**, *84*, 241410. [CrossRef]
15. Kikuzuki, T.; Lippmaa, M. Characterizing a strain-driven phase transition in VO_2. *Appl. Phys. Lett.* **2010**, *96*, 132107. [CrossRef]
16. Gea, L.A.; Boatner, L. Optical switching of coherent VO_2 precipitates formed in sapphire by ion implantation and annealing. *Appl. Phys. Lett.* **1996**, *68*, 3081–3083. [CrossRef]
17. Wu, C.; Feng, F.; Feng, J.; Dai, J.; Peng, L.; Zhao, J.; Yang, J.; Si, C.; Wu, Z.; Xie, Y. Hydrogen-incorporation stabilization of metallic VO_2 (R) phase to room temperature, displaying promising low-temperature thermoelectric effect. *J. Am. Chem. Soc.* **2011**, *133*, 13798–13801. [CrossRef]
18. Xie, J.; Wu, C.; Hu, S.; Dai, J.; Zhang, N.; Feng, J.; Yang, J.; Xie, Y. Ambient rutile VO_2(R) hollow hierarchitectures with rich grain boundaries from new-state nsutite-type VO_2, displaying enhanced hydrogen adsorption behavior. *Phys. Chem. Chem. Phys.* **2012**, *14*, 4810–4816. [CrossRef]
19. Yoon, H.; Choi, M.; Lim, T.-W.; Kwon, H.; Ihm, K.; Kim, J.K.; Choi, S.-Y.; Son, J. Reversible phase modulation and hydrogen storage in multivalent VO_2 epitaxial thin films. *Nat. Mater.* **2016**, *15*, 1113–1119. [CrossRef]
20. Hu, B.; Ding, Y.; Chen, W.; Kulkarni, D.; Shen, Y.; Tsukruk, V.V.; Wang, Z.L. External-strain induced insulating phase transition in VO_2 nanobeam and its application as flexible strain sensor. *Adv. Mater.* **2010**, *22*, 5134–5139. [CrossRef]

21. Liu, N.; Mesch, M.; Weiss, T.; Hentschel, M.; Giessen, H. Infrared perfect absorber and its application as plasmonic sensor. *Nano Lett.* **2010**, *10*, 2342–2348. [CrossRef] [PubMed]
22. Anker, J.N.; Hall, W.P.; Lyandres, O.; Shah, N.C.; Zhao, J.; Van Duyne, R.P. Biosensing with plasmonic nanosensors. *Nat. Mater.* **2008**, *7*, 442–453. [CrossRef] [PubMed]
23. Sengupta, S.; Wang, K.; Liu, K.; Bhat, A.K.; Dhara, S.; Wu, J.; Deshmukh, M.M. Field-effect modulation of conductance in VO_2 nanobeam transistors with HfO_2 as the gate dielectric. *Appl. Phys. Lett.* **2011**, *99*, 062114. [CrossRef]
24. Kim, H.-T.; Chae, B.-G.; Youn, D.-H.; Maeng, S.-L.; Kim, G.; Kang, K.-Y.; Lim, Y.-S. Mechanism and observation of Mott transition in VO_2-based two-and three-terminal devices. *N. J. Phys.* **2004**, *6*, 52. [CrossRef]
25. Zhou, Y.; Ramanathan, S. Relaxation dynamics of ionic liquid—VO_2 interfaces and influence in electric double-layer transistors. *J. Appl. Phys* **2012**, *111*, 084508. [CrossRef]
26. Liu, M.; Hwang, H.Y.; Tao, H.; Strikwerda, A.C.; Fan, K.; Keiser, G.R.; Sternbach, A.J.; West, K.G.; Kittiwatanakul, S.; Lu, J. Terahertz-field-induced insulator-to-metal transition in vanadium dioxide metamaterial. *Nature* **2012**, *487*, 345–348. [CrossRef]
27. Schurig, D.; Mock, J.J.; Justice, B.; Cummer, S.A.; Pendry, J.B.; Starr, A.F.; Smith, D.R. Metamaterial electromagnetic cloak at microwave frequencies. *Science* **2006**, *314*, 977–980. [CrossRef]
28. Lee, C.-W.; Choi, H.J.; Jeong, H. Tunable metasurfaces for visible and SWIR applications. *Nano Converg.* **2020**, *7*, 1–11. [CrossRef]
29. Lu, J.; Liu, H.; Deng, S.; Zheng, M.; Wang, Y.; van Kan, J.A.; Tang, S.H.; Zhang, X.; Sow, C.H.; Mhaisalkar, S.G. Highly sensitive and multispectral responsive phototransistor using tungsten-doped VO_2 nanowires. *Nanoscale* **2014**, *6*, 7619–7627. [CrossRef]
30. Babulanam, S.; Eriksson, T.; Niklasson, G.; Granqvist, C. Thermochromic VO_2 films for energy-efficient windows. *Sol. Energy Mater.* **1987**, *16*, 347–363. [CrossRef]
31. Kamalisarvestani, M.; Saidur, R.; Mekhilef, S.; Javadi, F. Performance, materials and coating technologies of thermochromic thin films on smart windows. *Renew. Sust. Energ. Rev.* **2013**, *26*, 353–364. [CrossRef]
32. Lampert, C.M. Large-area smart glass and integrated photovoltaics. *Sol. Energy Mater. Sol. Cells* **2003**, *76*, 489–499. [CrossRef]
33. Lin, S.; Bai, X.; Wang, H.; Wang, H.; Song, J.; Huang, K.; Wang, C.; Wang, N.; Li, B.; Lei, M. Roll-to-roll production of transparent silver-nanofiber-network electrodes for flexible electrochromic smart Windows. *Adv. Mater.* **2017**, *29*, 1703238. [CrossRef]
34. Kim, M.-J.; Sung, G.; Sun, J.-Y. Stretchable and reflective displays: Materials, technologies and strategies. *Nano Converg.* **2019**, *6*, 1–24. [CrossRef]
35. Chen, Y.; Ai, B.; Wong, Z.J. Soft optical metamaterials. *Nano Converg.* **2020**, *7*, 1–17. [CrossRef]
36. Hoffmann, S.; Lee, E.S.; Clavero, C. Examination of the technical potential of near-infrared switching thermochromic windows for commercial building applications. *Sol. Energy Mater. Sol. Cells* **2014**, *123*, 65–80. [CrossRef]
37. Chang, T.; Cao, X.; Long, Y.; Luo, H.; Jin, P. How to properly evaluate and compare the thermochromic performance of VO_2-based smart coatings. *J. Mater. Chem. A* **2019**, *7*, 24164–24172. [CrossRef]
38. Li, M.; Magdassi, S.; Gao, Y.; Long, Y. Hydrothermal synthesis of VO_2 polymorphs: Advantages, challenges and prospects for the application of energy efficient smart windows. *Small* **2017**, *13*, 1701147. [CrossRef] [PubMed]
39. Li, S.-Y.; Niklasson, G.A.; Granqvist, C.-G. Thermochromic fenestration with VO_2-based materials: Three challenges and how they can be met. *Thin Solid Films* **2012**, *520*, 3823–3828. [CrossRef]
40. Saeli, M.; Piccirillo, C.; Parkin, I.P.; Binions, R.; Ridley, I. Energy modelling studies of thermochromic glazing. *Energy Build.* **2010**, *42*, 1666–1673. [CrossRef]
41. Majid, S.; Sahu, S.; Ahad, A.; Dey, K.; Gautam, K.; Rahman, F.; Behera, P.; Deshpande, U.; Sathe, V.; Shukla, D. Role of VV dimerization in the insulator-metal transition and optical transmittance of pure and doped VO_2 thin films. *Phys. Rev. B* **2020**, *101*, 014108. [CrossRef]
42. Zhao, L.; Miao, L.; Liu, C.; Li, C.; Asaka, T.; Kang, Y.; Iwamoto, Y.; Tanemura, S.; Gu, H.; Su, H. Solution-processed VO_2-SiO_2 composite films with simultaneously enhanced luminous transmittance, solar modulation ability and anti-oxidation property. *Sci. Rep.* **2014**, *4*, 1–11. [CrossRef]
43. Whittaker, L.; Wu, T.-L.; Patridge, C.J.; Sambandamurthy, G.; Banerjee, S. Distinctive finite size effects on the phase diagram and metal–insulator transitions of tungsten-doped vanadium (iv) oxide. *J. Mater. Chem.* **2011**, *21*, 5580–5592. [CrossRef]
44. Xu, Y.; Huang, W.; Shi, Q.; Zhang, Y.; Song, L.; Zhang, Y. Synthesis and properties of Mo and W ions co-doped porous nano-structured VO_2 films by sol–gel process. *J. Solgel Sci. Technol.* **2012**, *64*, 493–499. [CrossRef]
45. Gao, Y.; Cao, C.; Dai, L.; Luo, H.; Kanehira, M.; Ding, Y.; Wang, Z.L. Phase and shape controlled VO_2 nanostructures by antimony doping. *Energy Environ. Sci.* **2012**, *5*, 8708–8715. [CrossRef]
46. Griffiths, C.; Eastwood, H. Influence of stoichiometry on the metal-semiconductor transition in vanadium dioxide. *J. Appl. Phys* **1974**, *45*, 2201–2206. [CrossRef]
47. Muraoka, Y.; Hiroi, Z. Metal–insulator transition of VO_2 thin films grown on TiO_2 (001) and (110) substrates. *Appl. Phys. Lett.* **2002**, *80*, 583–585. [CrossRef]
48. Dai, L.; Cao, C.; Gao, Y.; Luo, H. Synthesis and phase transition behavior of undoped VO_2 with a strong nano-size effect. *Sol. Energy Mater. Sol. Cells* **2011**, *95*, 712–715. [CrossRef]
49. Liang, S.; Shi, Q.; Zhu, H.; Peng, B.; Huang, W. One-step hydrothermal synthesis of W-doped VO_2 (M) nanorods with a tunable phase-transition temperature for infrared smart windows. *ACS Omega* **2016**, *1*, 1139–1148. [CrossRef] [PubMed]

50. Strelcov, E.; Tselev, A.; Ivanov, I.; Budai, J.D.; Zhang, J.; Tischler, J.Z.; Kravchenko, I.; Kalinin, S.V.; Kolmakov, A. Doping-based stabilization of the M_2 phase in free-standing VO_2 nanostructures at room temperature. *Nano Lett.* **2012**, *12*, 6198–6205. [CrossRef] [PubMed]
51. Panagopoulou, M.; Gagaoudakis, E.; Boukos, N.; Aperathitis, E.; Kiriakidis, G.; Tsoukalas, D.; Raptis, Y. Thermochromic performance of Mg-doped VO_2 thin films on functional substrates for glazing applications. *Sol. Energy Mater. Sol. Cells* **2016**, *157*, 1004–1010. [CrossRef]
52. Zhao, Z.; Liu, Y.; Wang, D.; Ling, C.; Chang, Q.; Li, J.; Zhao, Y.; Jin, H. Sn dopants improve the visible transmittance of VO_2 films achieving excellent thermochromic performance for smart window. *Sol. Energy Mater. Sol. Cells* **2020**, *209*, 110443. [CrossRef]
53. Patridge, C.J.; Whittaker, L.; Ravel, B.; Banerjee, S. Elucidating the Influence of Local Structure Perturbations on the Metal–Insulator Transitions of $V_{1-x}Mo_xO_2$ Nanowires: Mechanistic Insights from an X-ray Absorption Spectroscopy Study. *J. Phys. Chem. C* **2012**, *116*, 3728–3736. [CrossRef]
54. Li, D.; Li, M.; Pan, J.; Luo, Y.; Wu, H.; Zhang, Y.; Li, G. Hydrothermal synthesis of Mo-doped VO_2/TiO_2 composite nanocrystals with enhanced thermochromic performance. *ACS Appl. Mater. Interfaces* **2014**, *6*, 6555–6561. [CrossRef] [PubMed]
55. Dai, L.; Chen, S.; Liu, J.; Gao, Y.; Zhou, J.; Chen, Z.; Cao, C.; Luo, H.; Kanehira, M. F-doped VO_2 nanoparticles for thermochromic energy-saving foils with modified color and enhanced solar-heat shielding ability. *Phys. Chem. Chem. Phys.* **2013**, *15*, 11723–11729. [CrossRef] [PubMed]
56. Gao, Y.; Wang, S.; Luo, H.; Dai, L.; Cao, C.; Liu, Y.; Chen, Z.; Kanehira, M. Enhanced chemical stability of VO_2 nanoparticles by the formation of SiO_2/VO_2 core/shell structures and the application to transparent and flexible VO_2-based composite foils with excellent thermochromic properties for solar heat control. *Energy Environ. Sci.* **2012**, *5*, 6104–6110. [CrossRef]
57. Cui, Y.; Ke, Y.; Liu, C.; Chen, Z.; Wang, N.; Zhang, L.; Zhou, Y.; Wang, S.; Gao, Y.; Long, Y. Thermochromic VO_2 for energy-efficient smart windows. *Joule* **2018**, *2*, 1707–1746. [CrossRef]
58. Li, S.-Y.; Niklasson, G.A.; Granqvist, C.-G. Nanothermochromics: Calculations for VO_2 nanoparticles in dielectric hosts show much improved luminous transmittance and solar energy transmittance modulation. *J. Appl. Phys* **2010**, *108*, 063525. [CrossRef]
59. Ke, Y.; Balin, I.; Wang, N.; Lu, Q.; Tok, A.I.Y.; White, T.J.; Magdassi, S.; Abdulhalim, I.; Long, Y. Two-dimensional SiO_2/VO_2 photonic crystals with statically visible and dynamically infrared modulated for smart window deployment. *ACS Appl. Mater. Interfaces* **2016**, *8*, 33112–33120. [CrossRef]
60. Kang, L.; Gao, Y.; Luo, H.; Chen, Z.; Du, J.; Zhang, Z. Nanoporous thermochromic VO_2 films with low optical constants, enhanced luminous transmittance and thermochromic properties. *ACS Appl. Mater. Interfaces* **2011**, *3*, 135–138. [CrossRef]
61. Mlyuka, N.; Niklasson, G.A.; Granqvist, C.-G. Thermochromic multilayer films of VO_2 and TiO_2 with enhanced transmittance. *Sol. Energy Mater. Sol. Cells* **2009**, *93*, 1685–1687. [CrossRef]
62. Ke, Y.; Chen, J.; Lin, G.; Wang, S.; Zhou, Y.; Yin, J.; Lee, P.S.; Long, Y. Smart windows: Electro-, thermo-, mechano-, photochromics, and beyond. *Adv. Energy Mater.* **2019**, *9*, 1902066. [CrossRef]
63. Cao, X.; Chang, T.; Shao, Z.; Xu, F.; Luo, H.; Jin, P. Challenges and opportunities toward real application of VO_2-based smart glazing. *Matter* **2020**, *2*, 862–881. [CrossRef]
64. Chang, Q.; Wang, D.; Zhao, Z.; Ling, C.; Wang, C.; Jin, H.; Li, J. Size-Controllable M-Phase VO_2 Nanocrystals for Flexible Thermochromic Energy-Saving Windows. *ACS Appl. Nano Mater.* **2021**, *4*, 6778–6785. [CrossRef]
65. Gao, Y.; Wang, S.; Kang, L.; Chen, Z.; Du, J.; Liu, X.; Luo, H.; Kanehira, M. VO_2–Sb: SnO_2 composite thermochromic smart glass foil. *Energy Environ. Sci.* **2012**, *5*, 8234–8237. [CrossRef]
66. Choi, Y.; Sim, D.M.; Hur, Y.H.; Han, H.J.; Jung, Y.S. Synthesis of colloidal VO_2 nanoparticles for thermochromic applications. *Sol. Energy Mater. Sol. Cells* **2018**, *176*, 266–272. [CrossRef]
67. Manca, N.; Pellegrino, L.; Kanki, T.; Venstra, W.J.; Mattoni, G.; Higuchi, Y.; Tanaka, H.; Caviglia, A.D.; Marré, D. Selective high-frequency mechanical actuation driven by the VO_2 electronic instability. *Adv. Mater.* **2017**, *29*, 1701618. [CrossRef] [PubMed]
68. Warwick, M.E.; Ridley, I.; Binions, R. Thermochromic vanadium dioxide thin films prepared by electric field assisted atmospheric pressure chemical vapour deposition for intelligent glazing application and their energy demand reduction properties. *Sol. Energy Mater. Sol. Cells* **2016**, *157*, 686–694. [CrossRef]
69. Jiazhen, Y.; Yue, Z.; Wanxia, H.; Mingjin, T. Effect of Mo-W Co-doping on semiconductor-metal phase transition temperature of vanadium dioxide film. *Thin Solid Films* **2008**, *516*, 8554–8558. [CrossRef]
70. Warwick, M.E.; Binions, R. Thermochromic vanadium dioxide thin films from electric field assisted aerosol assisted chemical vapour deposition. *Sol. Energy Mater. Sol. Cells* **2015**, *143*, 592–600. [CrossRef]
71. Gagaoudakis, E.; Michail, G.; Aperathitis, E.; Kortidis, I.; Binas, V.; Panagopoulou, M.; Raptis, Y.S.; Tsoukalas, D.; Kiriakidis, G. Low temperature rf-sputtered thermochromic VO_2 films on flexible glass substrates. *Adv. Mater. Lett.* **2017**, *8*, 757–761. [CrossRef]
72. Bukhari, S.A.; Kumar, S.; Kumar, P.; Gumfekar, S.P.; Chung, H.-J.; Thundat, T.; Goswami, A. The effect of oxygen flow rate on metal–insulator transition (MIT) characteristics of vanadium dioxide (VO_2) thin films by pulsed laser deposition (PLD). *Appl. Surf. Sci* **2020**, *529*, 146995. [CrossRef]
73. Garry, G.; Durand, O.; Lordereau, A. Structural, electrical and optical properties of pulsed laser deposited VO2 thin films on R-and C-sapphire planes. *Thin Solid Films* **2004**, *453*, 427–430. [CrossRef]
74. Chae, J.-Y.; Lee, D.; Woo, H.-Y.; Kim, J.B.; Paik, T. Direct transfer of thermochromic tungsten-doped vanadium dioxide thin-films onto flexible polymeric substrates. *Appl. Surf. Sci* **2021**, *545*, 148937. [CrossRef]
75. Lee, W.S.; Jeon, S.; Oh, S.J. Wearable sensors based on colloidal nanocrystals. *Nano Converg.* **2019**, *6*, 1–13. [CrossRef] [PubMed]

76. Zhou, Y.; Huang, A.; Li, Y.; Ji, S.; Gao, Y.; Jin, P. Surface plasmon resonance induced excellent solar control for VO_2@SiO_2 nanorods-based thermochromic foils. *Nanoscale* **2013**, *5*, 9208–9213. [CrossRef]
77. Guo, D.; Ling, C.; Wang, C.; Wang, D.; Li, J.; Zhao, Z.; Wang, Z.; Zhao, Y.; Zhang, J.; Jin, H. Hydrothermal one-step synthesis of highly dispersed M-phase VO_2 nanocrystals and application to flexible thermochromic film. *ACS Appl. Mater. Interfaces* **2018**, *10*, 28627–28634. [CrossRef] [PubMed]
78. Cao, C.; Gao, Y.; Luo, H. Pure single-crystal rutile vanadium dioxide powders: Synthesis, mechanism and phase-transformation property. *J. Phys. Chem. C* **2008**, *112*, 18810–18814. [CrossRef]
79. Zhang, J.; He, H.; Xie, Y.; Pan, B. Theoretical study on the tungsten-induced reduction of transition temperature and the degradation of optical properties for VO_2. *J. Chem. Phys.* **2013**, *138*, 114705. [CrossRef]
80. Chen, Z.; Gao, Y.; Kang, L.; Cao, C.; Chen, S.; Luo, H. Fine crystalline VO_2 nanoparticles: Synthesis, abnormal phase transition temperatures and excellent optical properties of a derived VO_2 nanocomposite foil. *J. Mater. Chem. A* **2014**, *2*, 2718–2727. [CrossRef]
81. Parkin, I.P.; Manning, T.D. Intelligent thermochromic windows. *J. Chem. Educ.* **2006**, *83*, 393. [CrossRef]
82. Zhang, J.; Wang, J.; Yang, C.; Jia, H.; Cui, X.; Zhao, S.; Xu, Y. Mesoporous SiO_2/VO_2 double-layer thermochromic coating with improved visible transmittance for smart window. *Sol. Energy Mater. Sol. Cells* **2017**, *162*, 134–141. [CrossRef]
83. Howard, S.A.; Evlyukhin, E.; Páez Fajardo, G.; Paik, H.; Schlom, D.G.; Piper, L.F. Digital Tuning of the Transition Temperature of Epitaxial VO_2 Thin Films on MgF_2 Substrates by Strain Engineering. *Adv. Mater. Interfaces* **2021**, *8*, 2001790. [CrossRef]
84. Choi, Y.; Lee, D.; Song, S.; Kim, J.; Ju, T.S.; Kim, H.; Kim, J.; Yoon, S.; Kim, Y.; Phan, T.B. Correlation between Symmetry and Phase Transition Temperature of VO_2 Films Deposited on Al_2O_3 Substrates with Various Orientations. *Adv. Electron. Mater.* **2021**, *7*, 2000874. [CrossRef]
85. Yan, J.; Huang, W.; Zhang, Y.; Liu, X.; Tu, M. Characterization of preferred orientated vanadium dioxide film on muscovite (001) substrate. *Phys. Status Solidi A* **2008**, *205*, 2409–2412. [CrossRef]
86. Li, C.-I.; Lin, J.-C.; Liu, H.-J.; Chu, M.-W.; Chen, H.-W.; Ma, C.-H.; Tsai, C.-Y.; Huang, H.-W.; Lin, H.-J.; Liu, H.-L. Van der Waal epitaxy of flexible and transparent VO_2 film on muscovite. *Chem. Mater.* **2016**, *28*, 3914–3919. [CrossRef]
87. Geim, A.K.; Grigorieva, I.V. Van der Waals heterostructures. *Nature* **2013**, *499*, 419–425. [CrossRef]
88. Novoselov, K.; Mishchenko, O.A.; Carvalho, O.A.; Neto, A.C. 2D materials and van der Waals heterostructures. *Science* **2016**, *353*, aac9439. [CrossRef]
89. Liu, Y.; Huang, Y.; Duan, X. Van der Waals integration before and beyond two-dimensional materials. *Nature* **2019**, *567*, 323–333. [CrossRef]
90. Liang, W.; Jiang, Y.; Guo, J.; Li, N.; Qiu, W.; Yang, H.; Ji, Y.; Luo, S.N. Van der Waals heteroepitaxial VO_2/mica films with extremely low optical trigger threshold and large THz field modulation depth. *Adv. Opt. Mater.* **2019**, *7*, 1900647. [CrossRef]
91. Wang, J.N.; Xiong, B.; Peng, R.W.; Li, C.Y.; Hou, B.Q.; Chen, C.W.; Liu, Y.; Wang, M. Flexible Phase Change Materials for Electrically-Tuned Active Absorbers. *Small* **2021**, *17*, 2101282. [CrossRef]
92. Chen, Y.; Fan, L.; Fang, Q.; Xu, W.; Chen, S.; Zan, G.; Ren, H.; Song, L.; Zou, C. Free-standing SWNTs/VO_2/Mica hierarchical films for high-performance thermochromic devices. *Nano Energy* **2017**, *31*, 144–151. [CrossRef]
93. Xiao, L.; Ma, H.; Liu, J.; Zhao, W.; Jia, Y.; Zhao, Q.; Liu, K.; Wu, Y.; Wei, Y.; Fan, S. Fast adaptive thermal camouflage based on flexible VO_2/graphene/CNT thin films. *Nano Lett.* **2015**, *15*, 8365–8370. [CrossRef] [PubMed]
94. Chang, T.; Zhu, Y.; Huang, J.; Luo, H.; Jin, P.; Cao, X. Flexible VO_2 thermochromic films with narrow hysteresis loops. *Sol. Energy Mater. Sol. Cells* **2021**, *219*, 110799. [CrossRef]
95. Chang, T.; Cao, X.; Li, N.; Long, S.; Gao, X.; Dedon, L.R.; Sun, G.; Luo, H.; Jin, P. Facile and low-temperature fabrication of thermochromic Cr_2O_3/VO_2 smart coatings: Enhanced solar modulation ability, high luminous transmittance and UV-shielding function. *ACS Appl. Mater. Interfaces* **2017**, *9*, 26029–26037. [CrossRef]
96. Martins, L.G.; Song, Y.; Zeng, T.; Dresselhaus, M.S.; Kong, J.; Araujo, P.T. Direct transfer of graphene onto flexible substrates. *Proc. Natl. Acad. Sci. USA* **2013**, *110*, 17762–17767. [CrossRef]
97. Malarde, D.; Powell, M.J.; Quesada-Cabrera, R.; Wilson, R.L.; Carmalt, C.J.; Sankar, G.; Parkin, I.P.; Palgrave, R.G. Optimized atmospheric-pressure chemical vapor deposition thermochromic VO_2 thin films for intelligent window applications. *ACS Omega* **2017**, *2*, 1040–1046. [CrossRef]
98. Kim, H.; Kim, Y.; Kim, K.S.; Jeong, H.Y.; Jang, A.-R.; Han, S.H.; Yoon, D.H.; Suh, K.S.; Shin, H.S.; Kim, T. Flexible thermochromic window based on hybridized VO_2/graphene. *ACS Nano* **2013**, *7*, 5769–5776. [CrossRef]
99. Paik, T.; Hong, S.-H.; Gaulding, E.A.; Caglayan, H.; Gordon, T.R.; Engheta, N.; Kagan, C.R.; Murray, C.B. Solution-processed phase-change VO_2 metamaterials from colloidal vanadium oxide (VO_x) nanocrystals. *ACS Nano* **2014**, *8*, 797–806. [CrossRef] [PubMed]
100. Parameswaran, C.; Gupta, D. Large area flexible pressure/strain sensors and arrays using nanomaterials and printing techniques. *Nano Converg.* **2019**, *6*, 1–23. [CrossRef]
101. Wang, S.; Liu, M.; Kong, L.; Long, Y.; Jiang, X.; Yu, A. Recent progress in VO_2 smart coatings: Strategies to improve the thermochromic properties. *Prog. Mater. Sci.* **2016**, *81*, 1–54. [CrossRef]
102. Chae, B.-G.; Kim, H.-T.; Yun, S.-J.; Kim, B.-J.; Lee, Y.-W.; Youn, D.-H.; Kang, K.-Y. Highly oriented VO_2 thin films prepared by sol-gel deposition. *Electrochem. Solid-State Lett.* **2005**, *9*, C12. [CrossRef]

103. Speck, K.; Hu, H.-W.; Sherwin, M.; Potember, R. Vanadium dioxide films grown from vanadium tetra-isopropoxide by the sol-gel process. *Thin Solid Films* **1988**, *165*, 317–322. [CrossRef]
104. Cao, X.; Wang, N.; Law, J.Y.; Loo, S.C.J.; Magdassi, S.; Long, Y. Nanoporous thermochromic VO_2 (M) thin films: Controlled porosity, largely enhanced luminous transmittance and solar modulating ability. *Langmuir* **2014**, *30*, 1710–1715. [CrossRef] [PubMed]
105. Jo, Y.-R.; Lee, W.-J.; Yoon, M.-H.; Kim, B.-J. In Situ Tracking of Low-Temperature VO_2 Crystallization via Photocombustion and Characterization of Phase-Transition Reliability on Large-Area Flexible Substrates. *Chem. Mater.* **2020**, *32*, 4013–4023. [CrossRef]
106. Zhang, J.; Jin, H.; Chen, Z.; Cao, M.; Chen, P.; Dou, Y.; Zhao, Y.; Li, J. Self-assembling VO_2 nanonet with high switching performance at wafer-scale. *Chem. Mater.* **2015**, *27*, 7419–7424. [CrossRef]
107. Zhong, L.; Luo, Y.; Li, M.; Han, Y.; Wang, H.; Xu, S.; Li, G. TiO_2 seed-assisted growth of VO_2 (M) films and thermochromic performance. *CrystEngComm* **2016**, *18*, 7140–7146. [CrossRef]
108. Makarevich, A.; Makarevich, O.; Ivanov, A.; Sharovarov, D.; Eliseev, A.; Amelichev, V.; Boytsova, O.; Gorodetsky, A.; Navarro-Cia, M.; Kaul, A. Hydrothermal epitaxy growth of self-organized vanadium dioxide 3D structures with metal–insulator transition and THz transmission switch properties. *CrystEngComm* **2020**, *22*, 2612–2620. [CrossRef]
109. Guo, D.; Zhao, Z.; Li, J.; Zhang, J.; Zhang, R.; Wang, Z.; Chen, P.; Zhao, Y.; Chen, Z.; Jin, H. Symmetric confined growth of superstructured vanadium dioxide nanonet with a regular geometrical pattern by a solution approach. *Cryst. Growth Des.* **2017**, *17*, 5838–5844. [CrossRef]
110. Melnik, V.; Khatsevych, I.; Kladko, V.; Kuchuk, A.; Nikirin, V.; Romanyuk, B. Low-temperature method for thermochromic high ordered VO2 phase formation. *Mater. Lett.* **2012**, *68*, 215–217. [CrossRef]
111. Ivanov, A.V.; Makarevich, O.N.; Boytsova, O.V.; Tsymbarenko, D.M.; Eliseev, A.A.; Amelichev, V.A.; Makarevich, A.M. Citrate-assisted hydrothermal synthesis of vanadium dioxide textured films with metal-insulator transition and infrared thermochromic properties. *Ceram. Int.* **2020**, *46*, 19919–19927. [CrossRef]
112. Zhao, Z.; Liu, Y.; Yu, Z.; Ling, C.; Li, J.; Zhao, Y.; Jin, H. Sn–W Co-doping Improves Thermochromic Performance of VO_2 Films for Smart Windows. *ACS Appl. Energy Mater* **2020**, *3*, 9972–9979. [CrossRef]
113. Théobald, F. Étude hydrothermale du système VO_2-VO_2, 5-H_2O. *J. Less-Common Met.* **1977**, *53*, 55–71. [CrossRef]
114. Shi, J.; Zhou, S.; You, B.; Wu, L. Preparation and thermochromic property of tungsten-doped vanadium dioxide particles. *Sol. Energy Mater. Sol. Cells* **2007**, *91*, 1856–1862. [CrossRef]
115. Liu, P.; Zhu, K.; Gao, Y.; Wu, Q.; Liu, J.; Qiu, J.; Gu, Q.; Zheng, H. Ultra-long VO_2 (A) nanorods using the high-temperature mixing method under hydrothermal conditions: Synthesis, evolution and thermochromic properties. *CrystEngComm* **2013**, *15*, 2753–2760. [CrossRef]
116. Liu, L.; Cao, F.; Yao, T.; Xu, Y.; Zhou, M.; Qu, B.; Pan, B.; Wu, C.; Wei, S.; Xie, Y. New-phase VO_2 micro/nanostructures: Investigation of phase transformation and magnetic property. *New J. Chem.* **2012**, *36*, 619–625. [CrossRef]
117. Wu, C.; Hu, Z.; Wang, W.; Zhang, M.; Yang, J.; Xie, Y. Synthetic paramontroseite VO_2 with good aqueous lithium–ion battery performance. *Chem. Commun.* **2008**, 3891–3893. [CrossRef]
118. Shen, N.; Chen, S.; Chen, Z.; Liu, X.; Cao, C.; Dong, B.; Luo, H.; Liu, J.; Gao, Y. The synthesis and performance of Zr-doped and W–Zr-codoped VO_2 nanoparticles and derived flexible foils. *J. Mater. Chem. A* **2014**, *2*, 15087–15093. [CrossRef]
119. Popuri, S.R.; Miclau, M.; Artemenko, A.; Labrugere, C.; Villesuzanne, A.; Pollet, M. Rapid hydrothermal synthesis of VO_2 (B) and its conversion to thermochromic VO_2 (M_1). *Inorg. Chem.* **2013**, *52*, 4780–4785. [CrossRef]
120. Corr, S.A.; Grossman, M.; Shi, Y.; Heier, K.R.; Stucky, G.D.; Seshadri, R. VO_2 (B) nanorods: Solvothermal preparation, electrical properties, and conversion to rutile VO_2 and V_2O_3. *J. Mater. Chem.* **2009**, *19*, 4362–4367. [CrossRef]
121. Sun, Y.; Jiang, S.; Bi, W.; Long, R.; Tan, X.; Wu, C.; Wei, S.; Xie, Y. New aspects of size-dependent metal-insulator transition in synthetic single-domain monoclinic vanadium dioxide nanocrystals. *Nanoscale* **2011**, *3*, 4394–4401. [CrossRef] [PubMed]
122. Zhong, L.; Li, M.; Wang, H.; Luo, Y.; Pan, J.; Li, G. Star-shaped VO_2 (M) nanoparticle films with high thermochromic performance. *CrystEngComm* **2015**, *17*, 5614–5619. [CrossRef]
123. Song, Z.; Zhang, L.; Xia, F.; Webster, N.A.; Song, J.; Liu, B.; Luo, H.; Gao, Y. Controllable synthesis of VO_2 (D) and their conversion to VO_2 (M) nanostructures with thermochromic phase transition properties. *Inorg. Chem. Front.* **2016**, *3*, 1035–1042. [CrossRef]
124. Li, M.; Ji, S.; Pan, J.; Wu, H.; Zhong, L.; Wang, Q.; Li, F.; Li, G. Infrared response of self-heating VO_2 nanoparticles film based on Ag nanowires heater. *J. Mater. Chem. A* **2014**, *2*, 20470–20473. [CrossRef]
125. Li, M.; Wu, X.; Li, L.; Wang, Y.; Li, D.; Pan, J.; Li, S.; Sun, L.; Li, G. Defect-mediated phase transition temperature of VO 2 (M) nanoparticles with excellent thermochromic performance and low threshold voltage. *J. Mater. Chem. A* **2014**, *2*, 4520–4523. [CrossRef]
126. Chen, R.; Miao, L.; Liu, C.; Zhou, J.; Cheng, H.; Asaka, T.; Iwamoto, Y.; Tanemura, S. Shape-controlled synthesis and influence of W doping and oxygen nonstoichiometry on the phase transition of VO_2. *Sci. Rep.* **2015**, *5*, 1–12. [CrossRef]
127. Narayan, J.; Bhosle, V. Phase transition and critical issues in structure-property correlations of vanadium oxide. *J. Appl. Phys* **2006**, *100*, 103524. [CrossRef]
128. Zeng, W.; Chen, N.; Xie, W. Research progress on the preparation methods for VO_2 nanoparticles and their application in smart windows. *CrystEngComm* **2020**, *22*, 851–869. [CrossRef]
129. Lopez, R.; Feldman, L.C.; Haglund Jr, R.F. Size-Dependent Optical Properties of VO_2 Nanoparticle Arrays. *Phys. Rev. Lett.* **2004**, *93*, 177403. [CrossRef]

130. Liu, Y.; Liu, J.; Li, Y.; Wang, D.; Ren, L.; Zou, K. Effect of annealing temperature on the structure and properties of vanadium oxide films. *Opt. Mater. Express* **2016**, *6*, 1552–1560. [CrossRef]
131. Zhang, H.; Wu, Z.; Wu, X.; Yang, W.; Jiang, Y. Transversal grain size effect on the phase-transition hysteresis width of vanadium dioxide films comprising spheroidal nanoparticles. *Vacuum* **2014**, *104*, 47–50. [CrossRef]
132. Alie, D.; Gedvilas, L.; Wang, Z.; Tenent, R.; Engtrakul, C.; Yan, Y.; Shaheen, S.E.; Dillon, A.C.; Ban, C. Direct synthesis of thermochromic VO_2 through hydrothermal reaction. *J. Solid State Chem.* **2014**, *212*, 237–241. [CrossRef]
133. Li, W.; Ji, S.; Sun, G.; Ma, Y.; Guo, H.; Jin, P. Novel VO_2 (M)–ZnO heterostructured dandelions with combined thermochromic and photocatalytic properties for application in smart coatings. *New J. Chem.* **2016**, *40*, 2592–2600. [CrossRef]
134. Ji, S.; Zhang, F.; Jin, P. Preparation of high performance pure single phase VO_2 nanopowder by hydrothermally reducing the V_2O_5 gel. *Sol. Energy Mater. Sol. Cells* **2011**, *95*, 3520–3526. [CrossRef]
135. Chen, R.; Miao, L.; Cheng, H.; Nishibori, E.; Liu, C.; Asaka, T.; Iwamoto, Y.; Takata, M.; Tanemura, S. One-step hydrothermal synthesis of $V_{1-x}W_xO_2$ (M/R) nanorods with superior doping efficiency and thermochromic properties. *J. Mater. Chem. A* **2015**, *3*, 3726–3738. [CrossRef]
136. Kim, J.B.; Lee, D.; Yeo, I.H.; Woo, H.Y.; Kim, D.W.; Chae, J.-Y.; Han, S.H.; Paik, T. Hydrothermal synthesis of monoclinic vanadium dioxide nanocrystals using phase-pure vanadium precursors for high-performance smart windows. *Sol. Energy Mater. Sol. Cells* **2021**, *226*, 111055. [CrossRef]
137. Dahiya, A.S.; Shakthivel, D.; Kumaresan, Y.; Zumeit, A.; Christou, A.; Dahiya, R. High-performance printed electronics based on inorganic semiconducting nano to chip scale structures. *Nano Converg.* **2020**, *7*, 1–25. [CrossRef] [PubMed]
138. Li, S.-Y.; Niklasson, G.A.; Granqvist, C.-G. Nanothermochromics with VO_2-based core-shell structures: Calculated luminous and solar optical properties. *J. Appl. Phys* **2011**, *109*, 113515. [CrossRef]
139. Shen, N.; Chen, S.; Wang, W.; Shi, R.; Chen, P.; Kong, D.; Liang, Y.; Amini, A.; Wang, J.; Cheng, C. Joule heating driven infrared switching in flexible VO_2 nanoparticle films with reduced energy consumption for smart windows. *J. Mater. Chem. A* **2019**, *7*, 4516–4524. [CrossRef]
140. Zhou, J.; Gao, Y.; Liu, X.; Chen, Z.; Dai, L.; Cao, C.; Luo, H.; Kanahira, M.; Sun, C.; Yan, L. Mg-doped VO_2 nanoparticles: Hydrothermal synthesis, enhanced visible transmittance and decreased metal–insulator transition temperature. *Phys. Chem. Chem. Phys.* **2013**, *15*, 7505–7511. [CrossRef]
141. Nam, V.B.; Giang, T.T.; Koo, S.; Rho, J.; Lee, D. Laser digital patterning of conductive electrodes using metal oxide nanomaterials. *Nano Converg.* **2020**, *7*, 1–17. [CrossRef]
142. Yang, S.; Vaseem, M.; Shamim, A. Fully inkjet-printed VO_2-based radio-frequency switches for flexible reconfigurable components. *Adv. Mater. Technol.* **2019**, *4*, 1800276. [CrossRef]
143. Ji, H.; Liu, D.; Cheng, H.; Zhang, C. Inkjet printing of vanadium dioxide nanoparticles for smart windows. *J. Mater. Chem. C* **2018**, *6*, 2424–2429. [CrossRef]
144. Ji, H.; Liu, D.; Cheng, H.; Tao, Y. Large area infrared thermochromic VO_2 nanoparticle films prepared by inkjet printing technology. *Sol. Energy Mater. Sol. Cells* **2019**, *194*, 235–243. [CrossRef]
145. Wang, Y.; Zhao, F.; Wang, J.; Khan, A.R.; Shi, Y.; Chen, Z.; Zhang, K.; Li, L.; Gao, Y.; Guo, X. VO_2@SiO_2/Poly(N-isopropylacrylamide) hybrid nanothermochromic microgels for smart window. *Ind. Eng. Chem. Res.* **2018**, *57*, 12801–12808. [CrossRef]
146. Ji, H.; Liu, D.; Zhang, C.; Cheng, H. VO_2/ZnS core-shell nanoparticle for the adaptive infrared camouflage application with modified color and enhanced oxidation resistance. *Sol. Energy Mater. Sol. Cells* **2018**, *176*, 1–8. [CrossRef]
147. Wen, Z.; Ke, Y.; Feng, C.; Fang, S.; Sun, M.; Liu, X.; Long, Y. Mg-Doped VO_2@ZrO_2 Core—Shell Nanoflakes for Thermochromic Smart Windows with Enhanced Performance. *Adv. Mater. Interfaces* **2021**, *8*, 2001606. [CrossRef]
148. Saini, M.; Dehiya, B.S.; Umar, A. VO_2 (M)@CeO_2 core-shell nanospheres for thermochromic smart windows and photocatalytic applications. *Ceram. Int.* **2020**, *46*, 986–995. [CrossRef]
149. Moot, T.; Palin, C.; Mitran, S.; Cahoon, J.F.; Lopez, R. Designing Plasmon-Enhanced Thermochromic Films Using a Vanadium Dioxide Nanoparticle Elastomeric Composite. *Adv. Opt. Mater.* **2016**, *4*, 578–583. [CrossRef]